HHS Public Access

Author manuscript

Biomaterials. Author manuscript; available in PMC 2019 November 01.

Published in final edited form as:

Biomaterials. 2018 November ; 183: 280–294. doi:10.1016/j.biomaterials.2018.08.053.

Tumor Hypoxia Directed Multimodal Nanotherapy for Overcoming Drug Resistance in Renal Cell Carcinoma and Reprogramming Macrophages

Hashem O. Alsaab[#a,b], **Samaresh Sau**[#a,*], **Rami M. Alzhrani**[a,b], **Vino T. Cheriyan**[c], **Lisa A. Polin**[d,e], **Ulka Vaishampayan**[d], **Arun K. Rishi**[c,d,e,*], and **Arun K. Iyer**[a,f,*]

[a]Use-inspired Biomaterials & Integrated Nano Delivery (U-BiND) Systems Laboratory Department of Pharmaceutical Sciences, Eugene Applebaum College of Pharmacy and Health Sciences, Wayne State University, Detroit, MI 48201, USA

[b]Department of Pharmaceutics and Pharmaceutical Technology, College of Pharmacy, Taif University, Taif, 25671 Saudi Arabia.

[c]John D. Dingell VA Medical Center, Wayne State University, Detroit, Michigan, 48201, USA

[d]Department of Oncology, Karmanos Cancer Institute, Wayne State University School of Medicine, Detroit, Michigan, 48201, USA

[e]Molecular Therapeutics Program, Barbara Ann Karmanos Cancer Institute, Wayne State University, School of Medicine, Detroit, Michigan, 48201, USA

[f]Molecular Imaging Program, Barbara Ann Karmanos Cancer Institute, Wayne State University, School of Medicine, Detroit, Michigan, 48201, USA

[#] These authors contributed equally to this work.

Abstract

Drug resistance is one of the significant clinical burden in renal cell carcinoma (RCC). The development of drug resistance is attributed to many factors, including impairment of apoptosis, elevation of carbonic anhydrase IX (CA IX, a marker of tumor hypoxia), and infiltration of tumorigenic immune cells. To alleviate the drug resistance, we have used Sorafenib (Sor) in combination with tumor hypoxia directed nanoparticle (NP) loaded with a new class of apoptosis inducer, CFM 4.16 (C4.16), namely CA IX-C4.16. The NP is designed to selectively deliver the

[*]**Correspondence:** arun.iyer@wayne.edu, risha@karmanos.org or samaresh.sau@wayne.edu.

Author contributions

HA, SS, VTC, and RA performed the experiments; SS, AKR, and AKI conceived and designed the experiments; HA, and SS, AKR, and AKI analyzed data; and HA, SS, AKR, and AKI wrote the manuscript.

Declarations of interest

There are no conflicts to declare.

Data Availability Statement

The raw/processed data required to reproduce these findings cannot be shared at this time as the data also forms part of an ongoing study.

payload to the hypoxic tumor (core), provoke superior cell death in parental (WT) and Everolimus-resistant (Evr-res) RCC and selectively downmodulate tumorigenic M2-macrophage. Copper-free '*click*' chemistry was utilized for conjugating SMA-TPGS with Acetazolamide (ATZ, a CA IX-specific targeting ligand). The NP was further tagged with a clinically approved NIR dye (S0456) for evaluating hypoxic tumor core penetration and organ distribution. Imaging of tumor spheroid treated with NIR dye-labeled CA IX-SMA-TPGS revealed remarkable tumor core penetration that was modulated by CA IX-mediated targeting in hypoxic-A498 RCC cells. The significant cell killing effect with synergistic combination index (CI) of CA IX-C4.16 and Sor treatment suggests efficient reversal of Evr-resistance in A498 cells. The CA IX directed nanoplatform in combination with Sor has shown multiple benefits in overcoming drug resistance through (i) inhibition of p-AKT, (ii) upregulation of tumoricidal M1 macrophages resulting in induction of caspase 3/7 mediated apoptosis of Evr-res A498 cells in macrophage-RCC co-culturing condition, (iii) significant in vitro and in vivo Evr-res A498 tumor growth inhibition as compared to individual therapy, and (iv) untraceable liver and kidney toxicity in mice. Near-infrared (NIR) imaging of CA IX-SMA-TPGS-S0456 in Evr-res A498 RCC model exhibited significant accumulation of CAIX-oligomer in tumor core with >3-fold higher tumor uptake as compared to control. In conclusion, this proof-of-concept study demonstrates versatile tumor hypoxia directed nanoplatform that can work in synergy with existing drugs for reversing drug-resistance in RCC accompanied with re-education of tumor-associated macrophages, that could be applied universally for several hypoxic tumors.

Keywords

Renal Cell Carcinoma; overcoming drug resistance; macrophage modulation; Everolimus; tumor core penetration; nano-therapy; tumor hypoxia targeting; carbonic anhydrase IX

1. Introduction

Renal Cell Carcinoma (RCC) contributes to >90% of the most common form of kidney cancer and remains one of the ten leading causes of cancer deaths. It has been estimated that each year around 60,000 new patients are diagnosed with, and about 13,500 succumb to RCC [1]. Thus, RCC represents one of the most lethal malignant urological tumor [2]. The common form of RCC (more than 95%) is clear cell renal cell carcinoma (ccRCC) [3]. The mutation and inactivation of tumor suppressor Von Hippel-Lindau (VHL) gene is frequently observed in this malignancy that leads to a higher intracellular level of hypoxia-inducible factors 1α and 2α (HIF1α and HIF2α). The increased level of HIF-1α in RCC effectively regulates the tumorigenesis by upmodulating the function of AKT and VEGFR kinases that play an essential role in cellular metabolism, apoptosis inhibition, and hypoxia induction [4]. All these factors promote RCC to develop resistance to radiotherapy and conventional chemotherapy [5,6]. Several receptor tyrosine kinase inhibitors (TKIs), mammalian target of rapamycin inhibitors (mTOR) and serine-threonine kinase (STK) inhibitors are clinically approved for the treatment of RCC [7], although the benefit of overall progression-free survival remains poor (5-year survival rate of <10%). Thus, there is an urgent unmet need for targeted combination therapies with novel cell killing mechanisms [8,9]. Although, TKIs and mTOR inhibitors have increased therapeutic possibilities for treating RCC, a substantial

proportion of patients do not respond adequately, and therapy resistance almost inevitably occurs. Recently, new strategies have also emerged that include immunotherapy such as PD-1 inhibitor (Nivolumab) [10] and the combination of chemo-immune therapy [11]. These developments suggest that combination treatments aimed at different, non-related pathways could be advantageous [12–14]. In addition, due to the increase in vascular nature and high level of vascular permeability factor, ccRCC patients have benefited from anti-VEGFR cancer therapy. Over a period of time, the majority of the RCC patients ultimately develop a refractory response to anti-VEGFR treatment that is due to poor vascularization at the tumor core associated with tumor hypoxia[15]. In this regard, delivery of the therapeutic payload to the tumor hypoxic (core) is a rational approach for improving the current therapy. Additionally, development of novel synergistic therapeutic strategies, such as the resurrection of apoptosis, inhibition of AKT, and suppression of tumorigenic macrophages are desirable to tackle the current clinical challenges of drug-resistant and highly aggressive RCC [16]. We have developed Evr-res RCC cell model to evaluate the reversal of drug resistance using nano-combination therapy. We pursued different combination regimens, including drugs Evr (mTOR inhibitor) and Sorafenib (VEGFR and BRAF inhibitor).

The hypoxic tumor environment, highly prevalent in poorly vascularized and necrotic tumor core is well known to stimulate expression of VEGF and CA IX. CA IX is a membrane-bound protein that is overexpressed on the surface of many cancer cells in a hypoxic environment [17]. CA IX tightly controls the acid-base balance in the kidney [17], whereas during malignancy CA IX is involved in tumor cell survival and metastasis, and its increased expression correlates with poor clinical outcome. More than 7-clinical trials are underway to target CA IX in RCC and other solid tumors [NCT00059735, NCT00884520] that fortifies CA IX as an excellent biomarker for selective hypoxia mediated payload delivery. Numerous studies have investigated the CA IX distribution in normal tissues and malignancies [18–23]. Over-expression of CA IX has been documented in 93–97% of ccRCCs with rather low to limited expression in normal tissues/organs making it a selective biomarker for RCC [24]. Indeed, CA IX is almost homogeneously over-expressed in the ccRCC subtype [18–23,25,26]. Given the favorable tissue distribution, the potential of CA IX targeting of RCC for diagnosis or therapy has also been studied [27,28]. Due to the unique molecular attribute of RCC, CA IX is regarded as an excellent target for diagnosis and possibly for targeted therapy [20– 22,25,29]. Clinical trials have unambiguously demonstrated that CA IX can be targeted to RCC tissues with minimal damage to normal tissues, further highlighting suitable toxicity profiles of CA IX targeting [30,31]. However, there are no currently approved therapies against CA IX [32]. Monoclonal antibodies have been used to target CA IX, but their large molecular weight limits penetration through the poorly vascularized tumor and their slow blood clearance minimize their utilization as tumor imaging agents or radiotherapeutics because of high background and toxicity [31]. Finally, some recent studies have investigated whether small molecule CA IX-inhibitors can be used in serum assays or as an imaging target to monitor therapy responses [21–23]. Importantly, there is a critical need to develop safe and effective delivery vehicles that can carry the payload to the desired target tissue and cells [16,33–37].

Toward this end, we developed a simple and efficient multistage nanoplatform for systematically targeted polypharmacy payload delivery to induce the combination of

chemotherapeutic and immunotherapeutic effect in RCC. The oligomer we developed comprised of Vitamin-E- α-D-Tocopherol (TPGS) and styrene maleic anhydride (SMA) ligated with Acetazolamide (ATZ), namely CA IX-SMA-TPGS. The CA IX-SMA-TPGS oligomer was further encapsulated with C4.16 to obtain highly potent therapeutic payload containing nanoparticle CA IX-C4.16 respectively. The CA IX-C4.16 NPs have homogenous nanoparticle nature with narrow polydispersity index that is suitable for in vivo delivery. For ease of chemical synthesis of oligomers, we utilized copper free '*click*' chemistry. We have discovered and demonstrated CCAR1/CARP-1 protein as an inducer of apoptosis in RCC and other types of cancer. Upregulation of CARP-1 activates "apoptosis hallmarks", such as caspase mediated PARP cleavage, the downregulation of PI3K/AKT signaling and the loss of cyclin B1 in RCC[16]. To identify the potent activators of CARP-1, we developed a library of small molecule CARP-1 functional mimetic (CFM) compounds among them CFM4.16, namely C4.16, is highly efficient in RCC cell killing as obtained from NCI-60 screen [16]. Our data revealed that C4.16 is a superior inhibitor of both WT and Evr-resistant RCC cells with 4–5-fold improvement in IC50 value as compared to FDA approved Evr or Sor. In 2007, Sorafenib (Sor), a potent multi-kinase inhibitor of tumor-cell proliferation and angiogenesis, was clinically approved for oral treatment of advanced RCC with the median progression-free survival of 5.5 months [38]. Along with this encouraging clinical outcome, there are few reports on durable responses of Sor or the other VEGF pathway blockers. However, the majority of patients develop resistance to Sor within a median of 5–9 months [39]. Thus, more efficient and divergent combination therapy for inhibiting multiple tumorigenic pathways in RCC is required. Toward this, we found the combination of Sor and CA IX-C4.16 showed remarkable synergy in killing WT and Evr-res RCC cells. This combination treatment caused a complete wipeout of activated AKT (P-AKT) level, upregulated apoptosis hallmarks, such as caspase 3/7 and annexin V. The CA IX-C4.16+Sor is promising in upmodulating tumoricidal function of M-1 macrophage, while downmodulating tumorigenic M-2 macrophage associated biomarkers, such as CD206, arginase-1. Further, NIR imaging of CA IX-SMA-TPGS-S0456 confirmed the selective tumor accumulation of the vehicle with ~3-fold higher tumor as compared to control. The high intensity of NIR-dye in tumor core indicates selectivity of CA IX-SMA-TPGSS0456 in tumor hypoxia targeting. Finally, the significant tumor growth inhibition by CA IX-C4.16+Sor in Evr-res A498 model underscores the rationale of using Sor in combination nanotherapy as a promising platform in reversing drug resistance with untraceable liver and kidney toxicity (Scheme 1).

2. Materials and methods

2.1. Cell culture, reagents, and chemicals

Structure and synthesis of the C4.16 compound have been previously described [16,40]. A stock solution of 50 mM of C4.16 was solubilized in dimethyl sulfoxide (DMSO) and stored at –20°C for further use. Sor was obtained from LC Laboratories, Woburn, MA, and a 10 mM stock solution was prepared in DMSO and stored at –20°C. Everolimus (Evr) was obtained from selleckchem, Boston, MA, and a 10 mM stock solution were prepared in DMSO and stored at –20°C. Acetazolamide (ATZ), '*click*' chemistry reagents, Styrene maleic anhydride (SMA, MW 1600), D-alpha-tocopheryl polyethylene glycol succinate

(Vitamin E-TPGS), and 3-[4, 5-Dimethylthiazol-2-yl]-2, 5 diphenyltetrazolium bromide (MTT) were purchased from Sigma-Aldrich (St Louis, MO). NIR dye, S0456 was obtained from FEW Chemicals GmbH, Germany. We obtained all other analytical grade reagents from Fisher Scientific (Hampton, NH) and Sigma-Aldrich (St Louis, MO) and used them without further purification. DMEM, RPMI medium and antibiotics (penicillin and streptomycin) utilized in this work were purchased from Invitrogen Co. (Carlsbad, CA). Fetal bovine serum (FBS) and DMSO were purchased from Fisher Scientific (Fair Lawn, NJ). The Protein Assay Kit was obtained from Bio-Rad Laboratories (Hercules, CA). The rabbit monoclonal antibodies for β–actin was acquired from Sigma-Aldrich (St. Louis, MO). We purchased rabbit monoclonal antibodies to phospho- and total AKT, and Carbonic Anhydrase-IX (CA IX) from Cell Signaling Technology (Beverly, MA).,

2.2. Cell lines development and culturing condition

The human RCC A498 cells were from ATCC and kindly provided by Dr. Rajvir Dahiya (UCSF). All the cells were regularly maintained following procedures published before [41,42]. The cells were cultured in Dulbecco's modified Eagle's medium (DMEM) with GlutaMAX that was supplemented with 10% FBS, 100 units/ml of penicillin, and 100 μg/ml of streptomycin, and the cells were cultured at 37°C and 5% CO2. For cell viability and MTT studies, the cells were cultured in fresh media supplemented with 10% FBS before their treatments with various agents [43,44]. Resistant RCC cell-lines, including Evr-res A498, have been already established and validated in our previous work [16]. For inducing hypoxia, cells were treated with 200 μM Cobalt Chloride ($CoCl_2$) in standard growth media for 72 hrs before experiment [45,46]. RCC 3D-spheroid cell lines were grown in low density with 2% FBS containing culture media and before treatment they were induced with the hypoxic condition.

2.3. Preparation and Characterization of C4.16-loaded NP

After '*click*' reaction, we obtained CA IX-SMA-TPGS (CA IX-targeted oligomer), and in parallel, we generated SMA-TPGS (non-targeted oligomer). Both, (SMA-TPGS and CA IXSMA-TPGS-C4.16) NPs were developed using our previously reported methods with slight modification [16]. In brief, 100 mg of conjugated polymer was dissolved in 100 mL of deionized (DI) water under stirring. Then C4.16 (30 mg) was dissolved in 1 mL of DMSO and mixed with the polymer solution. Subsequently, 40 mg of EDC was added dropwise into solution and pH was kept at 5.0 to stir for 30 min. Then, the pH was raised to 11 and kept for other 30 min. Finally, pH was adjusted to 7.8 – 8.0 and the free drug C4.16 were removed by dialysis for 4–5 hrs in a bag with a cut-off of MW 2 kDa. Then, the products obtained were lyophilized to obtain the final powder and stored in the freezer until further use. Subsequently, the particle size and surface charge (zeta potential) measurements were performed using a Beckman Coulter Delsa Nano-C-DLS Particle analyzer (Miami, FL) equipped with a 658 nm He-Ne laser. For particle size, we suspended the NPs in DI water and detected the scattered light at 165° angle. We then obtained the peak average histograms of intensity, volume and number from 70 scans to calculate the average diameter of the particles. The zeta potentials were evaluated by measuring the electrophoretic mobility of the charged particles under an applied electric field. For Morphology, Transmission Electron Microscopy (TEM) of the NP was evaluated using JEOL-JEM-1000 instrument (JEOL Ltd,

Tokyo, Japan). We also characterized oligomer by proton nuclear magnetic resonance spectroscopy (^{1}H NMR) and Fourier transform infrared spectroscopy (FTIR). The structure of the synthesized SMA-TPGS and CA IX-SMA-TPGS copolymer was detected by ^{1}H NMR in D_2O as previously described [16][37]. The proper synthesis of the SMATPGS and CA IX-SMA-TPGS oligomer was also confirmed by the MALDI/MS and was found not to be a physical mixture of TPGS with SMA as all measurements indicated the absence of any free crystalline particles before NPs preparation.

2.4. The Drug loading (DLC) and encapsulation efficiency (EE) of C4.16 loaded-nanoparticles

We evaluated the C4.16 loading content percentage and the encapsulation efficiency (EE %) in NPs by High-Performance Liquid Chromatography (HPLC, Waters, Milford, MA). Samples of the C4.16 NPs preparations were taken, and the unentrapped C4.16 was quantified using our previously published HPLC method [16]. The loading efficiency of micelles was calculated by dissolving a known quantity of NPs directly in DMSO and further dilution of drugs with the mobile phase followed by determination of the absorbance at 309 nm (λ_{max}) with respect to the standard curve. Free drug (unentrapped C4.16 in the SMA-TPGS or CA IX-SMA-TPGS) was separated by ultrafiltration centrifugation technique. Briefly, 1 mL of CA IX-SMA-TPGS-C4.16 (targeted CA IX-C4.16 NPs) and SMA-TPGS-C4.16 (non-targeted) colloidal solutions were placed in the upper chamber of a centrifuge tube matched with an ultrafilter and centrifuged for 15 min at 4000 rpm. The total drug content in C4.16 NPs was determined as follows. Aliquots of 1 mL formulation dispersion were diluted accordingly by ethanol to dissolve the ingredient, and the resulting suspension was then filtrated through 0.45μm membrane filters. The filtered solution was analyzed by Waters® Alliance e2695 HPLC using Symmetry® C18 column (250mm × 4.6mm, 5μm). The mobile phase was a mixture of Acetonitrile, Methanol, 10 mM KH_2PO_4 buffer (65:20:15 v/v) with pH adjusted to 2, and the flow rate was maintained at 1.0 mL/min. All the samples were analyzed using empower PDA software. We then calculated the encapsulation efficiency (EE) and drug loading content (DLC) by the following equations:

$$\text{Drug loading content (DLC)} = \frac{\text{The weight of C}-4.16 \text{ encapsulated in micelles}}{\text{Total weight of C}-4.16 \text{ loaded in micelles}} \times 100 \quad \text{Equation (1)}$$

$$\text{Encapsulation Effeciency (EE)} = \frac{\text{Mass of C}-4.16 \text{ encapsulated in micelles}}{\text{Total mass of C}-4.16 \text{ initially loaded in micelles}} \times 100 \quad \text{Equation (2)}$$

2.5 Drug release kinetic study:

Drug release study was performed based on our previously published report[47]. Briefly, 200 μl of CAIX-C4.16 or C4.16 in Kolliphor in PBS pH 7.4 was placed in Thermo Scientific™ Slide-A-Lyzer™ 3.5K MWCO MINI Dialysis Devices with gentle agitation at 370C. The PBS solution outside the dialysis solution was collected at designated time and an equivalent volume of fresh PBS was compensated. The collected CDF contained was analyzed by HPLC and data was ploted as % cumulative drug release.

2.6 Expression of CA IX by A498 RCC cells and A498 RCC tumor models

The expression of CA IX on the surface of A498 and Evr-A498 cells was investigated under a normoxic or hypoxic condition by exposing cells to normoxia (no treatment) or hypoxia (cobalt chloride, $CoCl_2$ treatment) for 72 h, followed by CA IX detection using immunofluorescence analysis or western blot. Proteins from tumor tissues were extracted using RIPA buffer with the Halt Protease and Phosphatase Inhibitor Cocktail. A498 cells or tumors were fixed with 4% cold paraformaldehyde for 15 min after incubation for 24 h under normoxic or hypoxic condition. Cells were washed three times with DPBS and blocked with 10% bovine serum albumin for 1 h at room temperature, then incubated with primary rabbit monoclonal anti-CA IX antibody (20 μg/mL) overnight at 4°C. Cells were subsequently washed three times followed by incubation with FITC-conjugated rabbit anti-mouse secondary antibody for 1 h at room temperature. A498 cells under the normoxic or hypoxic condition, only treated with FITC-conjugated goat antimouse secondary antibody served as controls to avoid interference of cell auto-fluorescence. Cells were observed using a Confocal Laser Scanning Microscope (CLSM). For tumor tissues, mice were implanted with A498 cells using the technique previously reported [16]. Briefly, A498 cell suspensions were prepared in PBS and mice were injected with 1×10^6 cells subcutaneously by syringes with 29-gauge needles. On day 14 after tumor cell implantation, mice were sacrificed, and RCC tumor tissue was collected for histology performed by Biobank core facility.

2.7 Hypoxic core penetration of CA IX-SMA-TPGS oligomer in hypoxic A498 3D tumor spheroid

Cancer cell specific uptake of CA IX-SMA-TPGS oligomer was performed in tumor spheroids by immunofluorescence. Cells were cultured with ~70–80% confluence. We cultured Evr-res A498 cells to form 3D spheroid structure based on previously published

methods [16,40]. Briefly, the cells were washed twice in 1 × PBS, trypsinized and pelleted the cells with 200 ×g centrifugation at room temperature. It was re-suspended in 5 mL of sphere media (DMEM/F12 supplemented with 2 mM L-glutamine, 100 U/mL penicillin, 100 U/mL streptomycin, 1 × B27 supplement, 20ng/mL recombinant human epidermal growth factor (EGF; Sigma), and 10ng/mL recombinant human basic fibroblast growth factor (bFGF; R&D Systems). Cells were seeded approximately 5000 cells per mL on an ultra-low adherent 60mm plate and incubated at normal cell culturing conditions for two weeks without disturbing the plates. Seventy-two h prior to treatment, media was replaced with the hypoxic condition. Once the sphere was formed, spheres were treated with 1 μM Rhodamine B conjugated CA IX-SMA-TPGS oligomer (CA IX-RhodB) for 4 h or kept untreated at 37°C and 5% CO_2. At the end of the incubation period, the spheroids were washed with cold DPBS and scanned beginning from the top of the equatorial plane to obtain the Z-stack images by CLSM for the spheres of untreated and treated plates as described as reported before [48].

2.8 In vitro cytotoxicity assay

MTT assay was used to evaluate the anti-cancer effects of targeted CA IX-C4.16 NP and free anticancer drugs (C4.16, Evr, and Sor) in CA IX-positive (A498 RCC cells). First, the cells were seeded in a 96-well plate at a density of 5×10^3 cells per well and allowed to grow in fresh culture media overnight. Cells were subjected to parallel treatments under hypoxic and normoxic conditions as described above. After 20 h, the medium was removed, and the cells were washed twice with PBS. Cells were then treated with various concentrations of respective agents for the noted dose and time. Control cells were treated with 0.1% DMSO in the culture medium[49–51]. After treatment, cell viabilities were measured by the MTT assay. Briefly, 20 μl of 1mg/ml of MTT was added to each well and cells were incubated for 2–4 h at 37 °C. MTT was removed, and the resulting formazan products were dissolved by adding 50 μl DMSO/well followed by colorimetric analysis at 595 nm using a multi-label plate reader (Victor3; PerkinElmer, Wellesley, MA).

2.9 Western Blot analysis

The RCC cells were treated with DMSO/Vehicle (Control) or indicated dose and time of the noted compound. Cells were harvested and lysed in RIPA buffer (50 mM Tris-HCI, pH 8.0, 150 mM sodium chloride, 1.0% NP-40, 0.5% sodium deoxycholate, 0.1% sodium dodecyl sulphate (SDS), and 0.1% of protease inhibitor cocktail) for 20 min at 4°C. The lysates were then centrifuged at 14,000 rpm at 4 °C for 15 min to get rid of debris. We then determined the protein concentrations of whole cell lysates using the Bradford Protein Assay Kit. Supernatant proteins, 50μg from each sample, were separated by SDS-10% polyacrylamide gel electrophoresis (SDSPAGE) and transferred to polyvinylidene difluoride (PVDF) membrane (Bio-Rad, Hercules, CA) by standard procedures. The membranes were hybridized with primary antibodies followed by incubation with appropriate secondary antibodies. The antibody-bound proteins were visualized by treatment with the chemiluminescence detection reagent (Amersham Biosciences) according to the manufacturer’s instructions, followed by exposure to X-ray film (Kodak X-Omat). The same membranes were then re-probed with the anti-β actin antibody, which was used as an internal control for protein loading.

2.10 Apoptosis analysis by flow cytometry and Caspase 3/7 Glo assay

We determined apoptosis induction in A498 RCC cells that were treated with free C.4.16 or CA IX-C4.16 NP by flow cytometry with Annexin V/7-AAD dual staining. The percentage of Annexin V^{-}/7-AAD $^{-}$ (R5), Annexin V^{+}/7-AAD $^{-}$ (R6) and Annexin V^{-}/7-AAD $^{+}$ (R4) and Annexin V^{-}/7-AAD $^{+}$ (R3) cells were obtained to determine the number of live, as well as early and late apoptotic, and necrotic cells. To evaluate caspase-3/7 activities, cells were cultured and treated with DMEM medium (Free oligomer or control), C4.16, Sor, or C4.16+Sor for 24 h and were tested by Caspase-Glo 3/7 Assay (Promega) according to the manufacturer's recommendations.

2.11 Reprogramming macrophages with (CA IX-C4.16+Sor)

Transwell inserts 0.4 μM Corning, Falcon®, catalog number: 353493 and Corning® 6 well cell culture plates were used. Figure 6 A shows a diagram representing a brief outline of the steps of the protocol and a timeline indicating the order of events that were all carried out under sterile conditions following protocol published by Smith *et al.* Briefly, Raw264.7 cells were placed into the Transwell inserts. Raw-264.7 cells were first polarized to M1-macrophage using IFN-γ and LPS, and to M2-macrophage using IL-4 recombinant protein. Then, A498 RCC cell lines were cocultured with activated macrophages followed by treatment of Sor, C4.16, and CA IXC4.16+Sor for 24 h. Caspase 3/7 assay was performed in Evr-res A498 cells treated with Sor, C4.16, and CA IX-C4.16+Sor while co-culturing with Raw-264.7 macrophage to demonstrate whether combination treatment can reeducate macrophage to induce apoptosis mediated A498 cell death.

2.12 Antitumor therapy study in highly aggressive Evr-res A498 tumor in nu/nu xenograft model

The generation of RCC cell-derived subcutaneous tumor was done according to our previously published protocols approved by the Institutional Laboratory Animal Care & Use Committee (IACUC) at the Wayne State University [16,40]. Female, 5–6 weeks old nu/nu mice were obtained from Jackson Laboratory, Bar Harbor, ME. For therapy studies, after an appropriate period of acclimation, a suspension of 1×10^6 Evr-res A498 cells in 150 μl PBS was subcutaneously implanted in flanks of each animal using a 27-gauge needle. Tumors were allowed to grow for 10 days. When tumors became palpable (200 mm^3), the mice were randomly assigned for treatment or control groups of five animals each. Mice were treated with Vehicle (Control), CA IX-C4.16 NP (24 mg/kg/day), Sor (10 mg/kg/day) via intravenous (i.v) administration. Sor was formulated with 10% Kolliphor EL in PBS with DMSO concentration is <5%. In case of CA IX-C4.16 and Sor combination, only two doses were administered where the first dose was on day 1 was followed by the second dose on the third day. The tumor volume was measured, and mice were monitored for body weight changes. Antitumor activity was measured by using NIH formula, tumor volume (mm^3) = $1/2(\text{length} \times \text{width}^2)$. The tumor volume of the last day of therapy study was represented to demonstrate the endpoint outcome of combination therapy as described before [16]. The animals were sacrificed, and tumor tissues were collected. Representative tumor samples were stored at –80°C for subsequent analysis. The histology of normal organs (Kidney and Liver) was performed by Biobank core facility.

2.13 NIR imaging and bio-distribution of CA IX-SMA-TPGS-S0456 oligomer

A CA IX-targeted oligomer was conjugated with Near-infrared (NIR) dye CA IX-SMA-TPGSS0456, namely CA IX-S0456 (CA IX-oligomer) and administered via i.v route to 5–6 weeks old nu/nu mice, and the bio-distribution of NIR dye was monitored after 24 h of the single dose with 10 nmole NIR dye per mouse. Fluorescence images were collected in Bruker Carestream Xtreme in vivo imaging system at excitation (750 nm) and emission (830 nm) wavelength. The bio-distribution and tumor-targeting properties of CA IX-S0456 was evaluated after euthanizing the mice after 24 h post i.v injection. The instrument has dual fluorescence and X-ray imaging modalities with light source: 400 W Xenon illuminator. Both fluorescence and X-ray images of the mouse were merged to demonstrate the localization of NIR dye.

2.14 Statistical analysis

The statistical analyses were performed using Prism 7.0 software (Graph Pad Software Inc., San Dieg, CA). The data were expressed as mean ± SEM and analyzed using a two-tailed Student t-test or one-way ANOVA followed by a post hoc test unless specified otherwise. A p value of <0.05 was considered statistically significant.

3. Results and discussion

3.1. General procedure for synthesis of compound SMA-TPGS and ATZ-SMA-TPGS by Copper-free '*click*' chemistry

The current work aims to synthesize and formulate nanosystems targeting hypoxia in tumors. CA IX enzyme on the surface of kidney cancer cells was targeted by ATZ-containing oligomers using a modular copper-free *'click'* chemistry-based approach. As illustrated in Scheme 1 of Figure 1, we first synthesized acetazolamide-amine (ATZ-NH_2) from acetazolamide (ATZ) by acid hydrolysis as previously described [52]. Subsequently, ATZ-NH_2 was reacted with DBCONHS-ester to arrive at ATZ-DBCO (compound a) which functions as a CA IX targeting ligand. Second, in Scheme 2 of Figure 1, we synthesized SMA-TPGS oligomer (SMA-TPGS-Cys) by adding known amounts of TPGS and Cysteine in dichloromethane at pH 8 with fixed amounts of anhydrous SMA to permit its anhydride ring opening reaction with the alcohol group of TPGS and amine group of cystine. Then, we conjugated the SMA-TPGS-Cys with azido (N_3) group of (NH_2-PEG_8-N_3) compound by acid-amine coupling (EDC/NHS) reaction to finally get (compound b). Finally, the Copper-free '*click*' reaction was carried out by reacting compound 'a' with compound 'b' to form triazole ring, compound 'c'. All unconjugated reactants were removed by dialysis prior to lyophilization. The compound 'c' was reacted with Rhodamine B NCS to obtain "CA IX-Rhod" for in vitro 3D spheroid uptake study [53] and reacted with S0456 to get "CA IX-S0456" for in vivo tumor imaging [54]. S0456 is a near-infrared (NIR) fluorescent dye used in phase III clinical trials for image guided tumor surgery [55]. The final compounds were characterized by MALDI-MS, ^{1}H-NMR (Supplementary, S1 A-C) to assure chemical identity. ^{1}H-NMR results confirmed the triazole ring formation in CA IX-SMA-TPGS (Supplementary, S1 A, C) as the characteristic peaks were found for the -NH group of-triazole ring around δ7.9 ppm, O-CH_2 of triazole ring around 5.2, and CH_2-N_3 peak around 4.2 respectively. The molecules were analyzed by MALDI-MS spectroscopy to confirm the

chemical conjugation. This work expands upon our previous success in the design, synthesis, and development of SMA-TPGS-C4.16 and SMA-C4.16 nanomicellar formulation [16].

3.2. Preparation and characterization of CA IX targeting NP

The oligomers (SMA-TPGS and CA IX-SMA-TPGS) conjugate was purified by ultrafiltration (Millipore TFF, Milford, MA) and then lyophilized. The NPs were prepared with different methods, such as solvent evaporation, and oil-in-water emulsion method to formulate spherical micelles with SMA-TPGS and CA IX-SMA-TPGS. Both, CA IX targeted NP and non-targeted NP were loaded with water-insoluble C4.16 to produce CA IX-C4.16 NPs and SMA-TPGS-C4.16. The NPs were characterized for size, charge and drug loading and these parameters are presented in Table 1. The particle size of non-targeted C4.16 loaded NPs were ~105.2 nm with a Polydispersity index (PDI=0.165) (Figure 2A). Morphology of the NP was also assessed using Transmission Electron Microscopy (TEM) instrument (Figure 2 B) and the particle size resembled with DLS data and a favorable negative surface charge of NPs was noted (Figure 2C). After incorporation of targeting ligand (ATZ) to NPs, the particle size slightly increased compared to that of the non-targeted NPs suggesting the presence of ATZ on the surface of NPs. These results indicate that both the size and surface properties are optimal and safe for intravenous injection as well as ideal for tumor delivery. The Figure 2 C show histograms of comparative analyses of the particle size and zeta potential of the NPs. Figure 2 D indicates the results of MALDI-MS analysis of CA IX-SMA-TPGS and SMA-TPGS. The increment of molecular weight in CA IX-SMA-TPGS (m/z 3126) compared to SMA-TPGS (m/z 2399) and their corresponding fragmented peaks indicates the successful conjugation of ATZ to the SMATPGS polymers. Also, The C4.16 loading content and encapsulation efficiency in both NPs were evaluated by High-Performance Liquid Chromatography (HPLC). First, a method for analyzing drug content was developed and validated according to ICH guidelines [56]. We found that critical micellar concentration (CMC) of SMA-TPGS-C4.16 and SMA-C4.16 is 0.010 and 0.021 mg/ml respectively. The lower CMC value of SMA-TPGS-C4.16 could be attributed to the presence of TPGS[57], resulting in highly stable micelle formation(Figure 2E). This observation is consistent with our previously published work[47]. The sustained C4.16 release of CAIXSMA-TPGS-C4.16 indicates the efficient in vivo outcome. The CAIX-C4.16 micelles has shown good shelf life stability (Supplementarty Fig S3)[58]. The loading efficiency of micelles was then calculated by dissolving known quantity of NPs directly in DMSO followed by determination of the absorbance at 309 nm with respect to the standard curve performed by HPLC method. The encapsulation efficiency was 85 % and 75.5 % for SMA-TPGS NPs and CA IX-C-4.16 NPs, respectively.

3.3. Rationale for choosing CA IX protein for RCC therapy

In this study, we have shown that CA IX was overexpressed in A498 and Evr-res A498 RCC cells and tumor. In Figure 3A, immunohistochemistry of CA IX-positive A498 RCC tumor xenografts collected from tumor tissue section is shown. The intense bright green fluorescence indicates the presence of CA IX. In Figure 3B, Western blot data show levels of CA IX protein in A498 and Evr-res A498 RCC cells that were cultured under normoxic (no cobalt chloride treatment) or hypoxic conditions (treated with cobalt chloride for 72h). Together with immunohistological localization of CA IX in RCC tumor, the up-regulation of

CA IX expression in hypoxic WT and Evr-res A498 RCC cells in comparison to their respective, normoxic counterparts provides a rational strategy for delivering the payload into the hypoxic core of RCC tumor. Moreover, CA IX has been shown to be specifically overexpressed in 93 to 97% of both ccRCC and some papillary RCCs, with limited expression in normal tissues [59]. CA IX is also an important biomarker for RCC, and it plays a pivotal role in tumor progression, acidification, metastasis, and the intra-tumoral hypoxic condition. CA IX expression on the cell surface is associated with induction of tumor hypoxia through regulation of HIF1α. The clinicopathological analysis have supported the fact that overexpression of CA IX in RCC is linked to poor disease prognosis and resistance to chemo and immunotherapy. Many clinical trials are evaluating CA IX linked inhibitors or antibodies for monotherapy or diagnostic imaging. Recently, a small molecule, acetazolamide (ATZ), with high affinity (Kd~ 8.3 nM) to CA IX [60] has been reported to deliver the payload into the inner core (more than the periphery) of a tumor [52,54]. These results signify that CA IX is an excellent target for site-specific delivery of therapeutic payloads to renal tumors [61,62]. Along these lines, we developed ATZ-conjugated NPs for selective delivery of drug cocktail to the hypoxic region including the tumor core of therapy resistant RCC. It is well established that the hypoxic tumor core harbors aggressive and drug-resistant stem-like cells can persist after initial drug therapy, which can invade normal tissues and metastasize to distant sites forming secondary tumors. Targeting the hypoxic core using CA IX is thus a highly innovative approach needing immediate attention.

3.4. Selective uptake and tumor spheroid core penetration of CA IX oligomers to RCC.

The 3 D spheroid cell culture model is an in vivo mimetic study for testing NPs deep tumor core penetration ability. Thus, culturing A498 RCC cell lines with a spheroid model in hypoxic condition could be predictive of the tumor permeability of CA IX targeted NPs. In Figure 3C, we found that the rhodamine-conjugated ATZ oligomer (CA IX-Rhod) has deep tumor matrix penetration and superior uptake in hypoxic Evr-res A498 spheroid model. The cell uptake study of CA IX targeted NPs was performed using Evr- res A498 spheroid model followed by imaging of spheroid using confocal microscopy. Interestingly, Z-stacking from 10, 40, 60, and 100 μm in confocal microscopy of CA IX targeted oligomer-treated cells indicate that rhodamine-signal is significantly higher in the core of the spheroid than the periphery (Figure 3. C-D). Figure S4 A-B shows the confocal microscopy of non-targeted SMA-TPGS-Rhod-B. The figure indicates that the non-targeted formulation has low cellular uptake as compared to CAIX-Rhod-B. This data supports the need of CAIX targeting ligand in oligomer for improving the hypoxic tumor core penetration. This also is a strong indication that CA IX targeted oligomer can penetrate deep into the tumor spheroid and likely reached the hypoxic regions very efficiently. The highest fluorescence intensity at the center (as indicated by arrow) of 3D- plot (Figure 3 C) suggests that CA IX targeted oligomer efficiently reached the core of tumor spheroid. Also, in Figure 3 C, with the lower range of Z-stacking from 40–60 μm section (which is the core) has more fluorescence intensity than the periphery. Z-stacking of the spheroid at different sections from 10–100μm with CA IX targeted formulations also shows superior fluorescence intensity from 4060 μm sections representing organoid core. Figure 3 E showed the overall merged view of CA IX-Rhod-B oligomer with bright field and compared with untreated control. Figure 3 F shows

the overall shape of the spheroid from along the three dimensions (x, y, and z) as another way of representation to demonstrate spheroid core penetration.

3.5 C4.16 anti-cancer effect and Hypoxia targeting ability of CA IX NP

RCC is very difficult to treat as the cells are mostly resistant to many current therapies. Therefore, newer treatments including better ways of drug delivery are urgently needed to fight this malignant disease efficiently. Our previous work has demonstrated generation and characterization of RCC cells that are resistant to Evr, a frontline mTOR-targeted therapy, and revealed that a class of CARP-1 functional mimetic (CFM) compounds especially C-4.16 inhibited parental (WT) and Evr-res RCCs[16]. In this study, we utilized C-4.16 and current clinical anti-RCC therapeutics Sor and Evr. First, we determined cytotoxicity of individual drugs C4.16, Sor, and Evr in both A498 as shown in Figure 4. Our results from Figure 4 A, B indicated that C4.16 was more effective in inhibiting growth of WT and Evr-res A498 compared with Sor. Evr, however, did not inhibit growth of Evr-res A498 RCC cells as previously published [14]. In order to understand the safety of combination therapy, we performed the hemolysis assay using CAIX-C4.16 and combination of CAIX-C4.16+Sor. The data from Supplementary S5A-B indicate concentraions as high as 45.5 mM of C4.16 and combination of (45.5 μM C4.16 +17.4 μM Sor) have no significant effect in blood hemolysis[63]. We then clarified whether a combination of C4.16 and Sor were more effective when compared with individual treatment. In vitro cytotoxicity assay of C4.16 and Sor on Figure 4 A, B indicates C4.16 was more potent than FDA approved drug (Sor) and combining both drugs showed significantly lower the IC50 value. All the results indicate C4.16 and Sor inhibited viabilities of WT and Evr-res RCC cells, and C4.16 when combined with sor was more effective than C4.16 or Sor alone. However, C4.16's poor water solubility limits it's in vivo testing and clinical translation. We addressed the solubility and delivery concerns of C4.16 by utilizing a nanotechnology-based approach. Thus, encapsulation of C4.16 in NP and conjugating them with CA IX targeting oligomer was considered as a functional approach for resolving the challenges to deliver the compounds selectively to resistant RCC. The results as noted in Figure 4 C show that CA IX-C4.16 was more effective in inhibiting growth of A498 (WT and Evr-res) compared to Sor and Evr and supported that CA IX-C4.16 nano-formulation was more potent compared to FDA approved drugs. The table in Figure 4 D summarizes IC_{50} values for all drugs with the WT and Evr-res RCC cell lines. The data in Figure 4 C, D showed that CA IX-C4.16 was more effective in inhibiting growth of A498 (WT and Evr-res) compared to Sor and Evr and collectively indicate that CA IX-C4.16 was more potent compared to other drug options. Furthermore, to confirm the synergism, we utilized CompoSyn® software to evaluate the combination index (CI) value of C4.16 and Sor. As shown in Figure 4 E, C4.16 and Sor had CI value (less than 1) of 0.531 for A498 WT and 0.654 for Evr-Res, which indicated synergism between the two compounds. Figure 4F also demonstrated a combination of CA IX-C4.16 with Sor is synergistic in RCC cell killing as obtained from isobologram analysis. Thus, low dose of CA IX-C4.16 NP could potentially sensitize RCC cells for inhibition by Sor. Moreover, as shown in Figure S.6, a combination of 500 nM dose of CA IX-C4.16 with various doses of Sor further support their synergistic inhibition of RCC cells. A 500 nM dose of CA IX-C4.16 caused greater inhibition of RCC cell growth when combined with low doses of Sor (100, 200, 500 nM).

3.6 Mechanism of C4.16 for overcoming drug resistance

In this study, we determined how induction of apoptosis and inhibition of oncogenic survival signaling would reinforce the synergistic cell killing and reversal of drug resistance in WT and Evr-res A498 cells when treated with CA IX C4.16+Sor. As shown in Figure 5 A, we observed inhibition of AKT activation as indicated by downregulation of pAKT in C4.16 and Sor treatment compared to untreated control. We found that Evr-res RCC cells that were treated with C4.16 or Sor had a greater loss of AKT activities when compared with their WT cells treated with respective agents. Interestingly though, a combination of C4.16 and Sor completely abolished AKT activity (pAKT) in both the WT and resistant cells. Therefore, it is likely that superior RCC growth inhibition by C4.16 and Sor is in part due to suppression of oncogenic AKT activity. Moreover, C4.16 cytotoxicity was mediated by apoptosis induction (Figure 5 A) supporting our prior studies that have shown activation of apoptosis in C4.16 treated cells. Although, C4.16 or Sor induced caspase-3/7 activation, a significant upregulation of caspase-3/7 activity was noted in RCC cells treated with C4.16+Sor as compared to control (Figure 5 B). This finding was further supported by an increment of early and late apoptotic events in both WT and Evr-res A498 cells treated with CA IX-C4.16+Sor as compared to untreated control or CA IX-C4.16 (Figure 5 C). The fraction of cells that stained with Annexin V (+ve) or Annexin V (+ve) and 7-AAD (+ve) was higher in combination treatment than singular treatments as shown in Figure 5 D. In all the cases; combination always worked better than individual drugs in inhibiting RCC cells growth.

As shown previously, C4.16-dependent loss of RCC cell viability was due in part to reduced cyclin B1 levels, activation of pro-apoptotic, stress-activated protein kinases (SAPKs), and apoptosis [16]. Importantly, we also demonstrated that CARP-1 was a key player in inducing apoptosis and cell cycle arrest in the breast, lung and renal cancer cells [64,65]. The up-regulation of CARP-1 promotes activation of “apoptosis hallmarks,” such as caspase-mediated PARP cleavage, downregulation of PI3K/AKT signaling and loss of cyclin B1 in RCC [16]. To identify potent activators of CARP-1, a library of small molecules, namely CARP-1 functional mimetic (CFM) compounds were developed. An NCI-60 screening, as well as high throughput screening using various cancer cell lines, including WT and drug-resistant Evr-res RCC, resulted in the identification of several potent analogs. Our current results suggest that C4.16 is a superior inhibitor of both WT and drug-resistant RCC even in comparison to the FDA approved drugs, such as Ever and Sor. As RCC is highly vascularized, the use of drugs to inhibit RTK, such as VEGFR or HGF signaling is used as first-line therapies. Alongside, mTOR inhibitors, such as Evr were approved as second-line single agent therapy. All these kinase inhibitors are approved for single agent therapy. However, tumors eventually become resistant to therapy including RKT/mTOR inhibitors. Our findings suggest that the NPs formulations of the CARP-1 inducer (C4.16) will be a worthwhile strategy to provide multiple benefits such as(i) amenable for i.v. injection of CAIX-C4.16 leading to lowering of drug dose for in vivo therapy; (ii) higher stability and bioavailability of CAIX-C4.16; (iii) sustain drug release of CAIX-C4.16 as shown in Figure 2E, and reduced toxicity of CAIX-C4.16+Sor.

Literature reports and clinical experience have revealed that inhibiting RCC proliferation with drugs combination specific to different targets is superior to monotherapy approaches

[66]. However, such approaches tend to produce severe on-target and off-target toxicities [67]. To achieve the maximum therapeutic benefits and reduce the toxicity, we encapsulated anticancer drugs in CA IX-C4.16 NPs. This i.v. administrable NPs in combination with currently approved drugs is an excellent approach to precisely target the convergent pathways of RCC activity with resistant and tumor stroma features [68].

3.7 Reprogramming macrophages to modulate combination treatment:

To overcome the critical problem of current RCC treatment, we developed a tumor-penetrating nano-sized NP of spherical shape that can localize and penetrate tumor tissues efficiently and target tumor hypoxia to deliver the combination drug cocktail to shut down vital tumorigenic signaling while simultaneously reprogramming macrophages for better therapeutic efficacy. Several studies have identified the key players that are responsible for drug resistance and immune evasion leading to the poor prognosis of RCC. These players are categorized based on their specific roles that include (i) RTK-mTOR that regulates critical tumorigenic signaling for tumor survival, immune suppression, and stroma formation [11], (ii) impairment of intrinsic and extrinsic apoptotic signaling is an essential player of drug resistance [12]. Induction of CARP-1 protein has been well documented to induce apoptosis in cancer cells under the conditions of serum withdrawal or therapy stress [10, 13]. (iii) CA IX is a tumor hypoxia marker for the maintenance of extracellular acidosis and cancer stemness, thus facilitating tumor growth and metastases. More than seven clinical trials are underway to target CA IX in RCC and other solid tumors [NCT00059735, NCT00884520] [14]. The delivery system we have engineered here will be a promising addition to clinical translation for better RCC treatment. Figure 6A shows a schematic diagram as Raw264.7 cells were placed into the insert. Then, cells were polarized to M1-macrophage using IFN-γ and LPS, and to M2-macrophage using IL-4 recombinant protein. The change of morphology of Raw264.7 as shown in Figure 6 B supports the M1/M2 polarization of naïve Raw264.7 cells[69] followed by treatment with C4.16 and CA IXC4.16+Sor for 24 h. The data in Figure 6 C clearly demonstrate the up-modulation of the tumoricidal M1-macrophage marker (CD86, iNOS) and down-modulation of the tumorigenic M2-macrophage marker (CD206, Arginase I) compared to untreated (UT) control and C4.16. The macrophage reprogramming ability of CA IX-targeting NP builds a rational of using (CA IX-C4.16+Sor) as a potent antitumor immune-stimulatory agent of RCC. The treatment of CA IX+Sor to Evr-res A498 cells co-cultured with M1-macrophage resulted in the growth inhibition and change of morphology that could be due to tumoricidal M-1 macrophage mediated cell death of RCC cells as shown in Figure 6 D. Further to evaluate the macrophage induced RCC cell death, we analyzed up-modulation of caspase 3/7 in Evr-res A498 cell co-cultured with Raw 264.7 cell and treated with CA IX-C4.16+Sor or other treatments. The data from Figure 6E clearly confirmed combination is significantly better in inducing apoptosis as compared to control or individual treatments. The mechanism of immune-modulaiton of CAIXC4.16+Sor can be attributed to inhibition of tumorigenic kinases, such as p-AKT[70] and resurrection of apoptosis. As CAIX-C4.16+Sor treatment is very effective in inhibiting PAKT (Figure 5A), the treatment of (CAIX-C4.16+Sor) in Evr-res A498 and M1/M2 macrophage co-culture condition is down-modulating the secretion of inflammatory cytokines, resulting in down-modulation of tumorigenic M2 macrophage function and up-modulation of M1 macrophage function. Another, possible explanation of

immunomodulatory effect of (CAIX-C4.16+Sor) could be suppression PD-1/PDL-1 cross talk. Prior literature has indicated that macrophages have elevated expression of PD-1 receptor that interact with PDL-1 of cancer cells[71]. Thus, CAIX-C4.16+Sor treatment can be inhibiting the PD-1/PDL-1 interaction, resulting in immune resurrection in co-culture condition as seen in Fig 6. All these results demonstrate hypoxia targeting NP in combination with Sor is not only inducing chemotherapeutic effect but also reeducating macrophages to function as a tumoricidal agent, which could prove excellent for a combination of chemo-immune therapy to inhibit Evr-res RCC.

3.8 Superior tumor core penetration and high tumor uptake of CA IX oligomers in xenograft RCC model.

After optimizing the anticancer effect of CA IX-C4.16 at the cellular level, we performed NIR imaging in animals inoculated with RCC tumor model following administration of CA IX-S0456. The idea of performing NIR-imaging with CA IX-oligomer will provide several advantages including its use as (i) agent for tumor image guided RCC surgery in the clinic, as well as (ii) meaningful insights into the therapeutic outcome and safety of nanoformulation in RCC model. It is well known that clinically small molecule NIR imaging agents have excellent ability to distinguish the tumor lesion from healthy tissue in imaging-guided surgery as noted in NCT02317705 and NCT01778933 [72]. The results show CA IX-S0456 selectively home to the orthotopic subcutaneous Evr-res A498 tumor as compared to control (Figure 7 A and C). The bio-distribution (Bio-D) study in Figure 7 B validates the prominent tumor selectivity of CA IXS0456.. The tumor selectivity of CA IX-S0456 in drug resistant RCC model builds a foundation for widespread applicability of CA IX-S0456 in Evr-res RCC tumor model that builds a rational platform for further investigation towards clinical translation of this technology. Herein, the reasons of using CAIX-S0456 oligomer compared to oligomicelles for tumor imaging is due to the fact that (i) small molecular weight oligomer, will help achieve deep tumor stroma penetration, (ii) hydrophilic nature of oligomer will assist faster clearance/excretion via the kidneys and healthy organs, while being selectively retained in the hypoxic tumor[73]. In Figure 3, 3D spheroid uptake study of CA IX-rhodamine showed high localization of rhodamine in the core of the hypoxic Evr-res A498 spheroid. To ascertain core penetrating ability of CA IX-S0456 in a drug resistant tumor model, we performed 3 transverse sectioning of the isolated tumor after the bio-D study. Figure 7D confirmed that CA IX-S0446 is very efficient in penetrating the core of tumor that predominantly harbors hypoxia and drug resistant features. As shown in Figure 7E, more than 3-fold tumor ROI in CA IX-oligomer compared to control demonstrates the feasibility of CA IX-S0456 in clinical translation as an image-guided surgery tool. The findings in Figure 7F suggest the ROI is >2 fold in CA IX-S0456 treated tumor core as compared to tumor periphery. These results support a high binding affinity and specific tumor uptake, faster normal tissue clearance, and low non-specific organ uptake of CA IX-oligomer.

3.9 Tumor growth inhibition and excellent safety of CA IX-C4.16+Sor in Evr-res tumor.

After confirming the in vitro anticancer activity, we finally examined the antitumor effect of CA IX-C4.16 NP in combination with Sor, to demonstrate the efficacy of combination regimen in reversing Evr-resistance in RCC. The CA IX-C4.16 NPs formulation inhibited

the viability of WT and Evr-res A498 cells in vitro by stimulating various tumoricidal pathways including induction of apoptosis, downregulation of pAKT and up-modulation and education of M1macrophages. As shown in Figure 7G, CA IX-C4.16 significantly inhibited highly aggressive Evr-res A498 tumor in combination with Sor. The greater tumor growth inhibitory effect of CA IX-C4.16+Sor compared to control and individual treatments thus opens an avenue that CA IXC4.16 nano-therapy can resurrect Sor as a more efficient anticancer therapeutic agent. Importantly, CA IX-C4.16+Sor did not cause any necrosis or morphological changes in tissue architecture of normal organs such as kidneys and liver (Figure 7 J). The superior tumor penetration of CAIX-oligomer and efficient antitumor effect of CA IX-C4.16+Sor in different RCC tumor model underscore a viable strategy for developing a smart therapy against drug resistant tumors with high safety profile. The rational of choosing the combination of C4.16 and Sor is to target the divergent pathway of RCC. C4.15 works through upregulation of CARP-1 protein, which is an inducer of apoptosis[16]. Whereas, Sor is a multikinase inhibitor. Thus, treatment of C4.16 resurrects the apoptosis pathway and Sor inhibits the tumor survival kinase signaling, resulting in the synergistic induction of anticancer effect and reversal of drug resistance of RCC. The current findings can support the claim that CA IX-NPs loaded with anticancer payload can play a universal role in overcoming drug resistance and repurposing current drugs in a more efficient way.

4. Conclusions

In this study, we have demonstrated elevated expression of CA IX in RCC that qualifies its use as an excellent biomarker for targeted therapy and imaging. The combination of C4.16 and Sor have a superior synergistic cell killing in Evr-res RCC, which is due in part to activation of caspase 3/7 protein and complete eradication of oncogenic AKT activation. Combination of CA IX-C4.16 with Sor showed targeted delivery of payload in hypoxic tumor resulting in induction of multimodal anticancer effects including, the resurrection of apoptosis, reversal of drug resistance, and reprogramming of malfunction macrophages. This NP could have a direct impact on developing newer therapies for treating RCC. We found that CA IX-C4.16 NP is suitable for intravenous administration with superior tumor accumulation of CA IX-oligomer as compared to liver and demonstrated effective antitumor response in Evr-res A498 tumor. Due to small molecular size and ease of chemical functionalization, CA IX-oligomer can potentially be further explored for selective CA IX tumor targeting for the diagnostic use and RCC image-guided surgery in the clinical setting. The tumor spheroid uptake study has clearly demonstrated excellent tumor core penetrating ability of CA IX-targeting oligomer, which is a critical indicator of tumor stromal disruption leading to better therapy response and immune modulation. In conclusion, the synergistic therapeutic potential of CA IX-C4.16 and Sor combination and selective NIR imaging of the CA IX anchored oligomer portend their promising potential towards developing better therapeutics and diagnostic tools for clinical translation against deadliest drug resistant RCC.

Supplementary Material

Refer to Web version on PubMed Central for supplementary material.

Acknowledgments

The authors would like to acknowledge partial support for this work by Wayne State University start-up funding to AKI, and funds from the Department of Veterans Affairs Merit Review to AKR. HA and RA acknowledge the scholarship support from the College of Pharmacy at Taif University and Saudi Arabian Cultural Mission (SACM). TEM analysis using JEOL 2010 was supported by an NSF Award#0216084. AKI would like to acknowledge the Karmanos Cancer Institute and the Molecular Imaging Program for access to its core facilities. The Biobanking and Correlative Sciences Core is supported, in part, by NIH Center grant P30 CA022453 to the Karmanos Cancer Institute at Wayne State University.

References

[1]. Hsieh JJ, Purdue MP, Signoretti S, Swanton C, Albiges L, Schmidinger M, Heng DY, Larkin J, Ficarra V, Renal cell carcinoma, Nat. Publ. Gr 3 (2017) 1–19. doi:10.1038/nrdp.2017.9.

[2]. Cairns P, Renal cell carcinoma, Cancer Biomarkers. 9 (2011) 461–473. doi:10.3233/CBM-2011-0176.

[3]. Creighton CJ, Morgan M, Gunaratne PH, Wheeler DA, Gibbs RA, Gordon Robertson A, Chu A, Beroukhim R, Cibulskis K, Signoretti S, Vandin Hsin-Ta Wu F, Raphael BJ, Verhaak RGW, Tamboli P, Torres-Garcia W, Akbani R, Weinstein JN, Reuter V, Hsieh JJ, Rose Brannon A, Ari Hakimi A, Jacobsen A, Ciriello G, Reva B, Ricketts CJ, Marston Linehan W, Stuart JM, Kimryn Rathmell W, Shen H, Laird PW, Muzny D, Davis C, Xi L, Chang K, Kakkar N, Treviño LR, Benton S, Reid JG, Morton D, Doddapaneni H, Han Y, Lewis L, Dinh H, Kovar C, Zhu Y, Santibanez J, Wang M, Hale W, Kalra D, Getz G, Lawrence MS, Sougnez C, Carter SL, Sivachenko A, Lichtenstein L, Stewart C, Voet D Fisher Sheila, Gabriel Stacey B., Lander E, Schumacher Steve E., Tabak B, Saksena Gordon, Onofrio RC, Cherniack AD, Gentry Jeff, Ardlie K, Sougnez Carrie, Gabriel SB, Meyerson M, Chun H-JE, Mungall AJ, Sipahimalani P, Stoll D, Ally A, Balasundaram M, Butterfield YSN, Carlsen R, Carter C, Chuah E, Coope RJN, Dhalla N, Gorski S, Guin R, Hirst C, Hirst M, Holt RA, Lebovitz C, Lee D, Li HI, Mayo M, Moore RA, Pleasance E, Plettner P, Schein JE, Shafiei A, Slobodan JR, Tam A, Thiessen N, Varhol RJ, Wye N, Zhao Y, Birol I, Jones SJM, Marra MA, Auman JT, Tan D, Jones CD, Hoadley KA, Mieczkowski PA, Mose LE, Jefferys SR, Topal MD, Liquori C, Turman YJ, Shi Y, Waring S, Buda E, Walsh J, Wu J, Bodenheimer T, Hoyle AP, Simons JV, Soloway MG, Balu S, Parker JS, Neil Hayes D, Perou CM, Kucherlapati R, Park P, Triche T, Jr, Weisenberger DJ, Lai PH, Bootwalla MS, Maglinte DT, Mahurkar S, Berman BP, Van Den Berg DJ, Cope L, Baylin SB, Noble MS, DiCara D, Zhang H, Cho J, Heiman DI, Gehlenborg N, Mallard W, Lin P, Frazer S, Stojanov P, Liu Y, Zhou L, Kim J, Chin L, Vandin F, Wu H-T, Benz C, Yau C, Reynolds SM, Shmulevich I, Verhaak RGW, Vegesna R, Kim H, Zhang W, Cogdell D, Jonasch E, Ding Z, Lu Y, Zhang N, Unruh AK, Casasent TD, Wakefield C, Tsavachidou D, Mills GB, Schultz N, Antipin Y, Gao J, Cerami E, Gross B, Arman Aksoy B, Sinha R, Weinhold N, Onur Sumer S, Taylor BS, Shen R, Ostrovnaya I, Berger MF, Ladanyi M, Sander C, Fei SS, Stout A, Spellman PT, Rubin DL, Liu TT, Ng S, Paull EO, Carlin D, Goldstein T, Waltman P, Ellrott K, Zhu J, Haussler D, Xiao W, Shelton C, Gardner J, Penny R, Sherman M, Mallery D, Morris S, Paulauskis J, Burnett K, Shelton T, Kaelin WG, Choueiri T, Atkins MB, Curley E, Tickoo S, Thorne L, Boice L, Huang M, Fisher JC, Vocke CD, Peterson J, Worrell R, Merino MJ, Schmidt LS, Czerniak BA, Aldape KD, Wood CG, Boyd J, Weaver J, Iacocca MV, Petrelli N, Witkin G, Brown J, Czerwinski C, Huelsenbeck-Dill L, Rabeno B, Myers J, Morrison C, Bergsten J, Eckman J, Harr J, Smith C, Tucker K, Anne Zach L, Bshara W, Gaudioso C, Dhir R, Maranchie J, Nelson J, Parwani A, Potapova O, Fedosenko K, Cheville JC, Houston Thompson R, Mosquera JM, Rubin MA, Blute ML, Pihl T, Jensen M, Sfeir R, Kahn A, Chu A, Kothiyal P, Snyder E, Pontius J, Ayala B, Backus M, Walton J, Baboud J, Berton D, Nicholls M, Srinivasan D, Raman R, Girshik S, Kigonya P, Alonso S, Sanbhadti R, Barletta S, Pot D, Sheth M, Demchok JA, Davidsen T, Wang Z, Yang L, Tarnuzzer RW, Zhang J, Eley G, Ferguson ML, Mills Shaw KR, Guyer MS, Ozenberger BA, Sofia HJ., Comprehensive molecular characterization of clear cell renal cell carcinoma, Nature. 499 (2013) 43–49. doi:10.1038/nature12222. [PubMed: 23792563]

[4]. Guo H, German P, Bai S, Barnes S, Guo W, Qi X, Lou H, Liang J, Jonasch E, Mills GB, Ding Z. The PI3K/AKT Pathway and Renal Cell Carcinoma, J. Genet. Genomics 42 (2015) 343–353. doi:10.1016/j.jgg.2015.03.003. [PubMed: 26233890]

[5]. Strese S, Fryknäs M, Larsson R, Gullbo J, Effects of hypoxia on human cancer cell line chemosensitivity, BMC Cancer. 13 (2013) 331. doi:10.1186/1471-2407-13-331. [PubMed: 23829203]

[6]. Smaldone MC, Maranchie JK, Clinical implications of hypoxia inducible factor in renal cell carcinoma., Urol. Oncol 27 (2009) 238–245. doi:10.1016/j.urolonc.2007.12.001. [PubMed: 19414111]

[7]. Voss MH, Molina AM, Motzer RJ, MTOR inhibitors in advanced renal cell carcinoma, Hematol. Oncol. Clin. North Am 25 (2011) 835–852. doi:10.1016/j.hoc.2011.04.008. [PubMed: 21763970]

[8]. Zarrabi K, Fang C, Wu S, New treatment options for metastatic renal cell carcinoma with prior anti-angiogenesis therapy, J. Hematol. Oncol 10 (2017) 38. doi:10.1186/s13045-016-0374-y. [PubMed: 28153029]

[9]. Rini BI, Atkins MB, Resistance to targeted therapy in renal-cell carcinoma, Lancet Oncol. 10 (2009) 992–1000. doi:10.1016/S1470-2045(09)70240-2. [PubMed: 19796751]

[10]. Alsaab H, Sau S, Alzhrani R, PD-1 and PD-L1 Checkpoint Signaling Inhibition for Cancer Immunotherapy: Mechanism, Combinations, and Clinical Outcome, Front. (2017).

[11]. Juengel E, Maxeiner S, Rutz J, Justin S, Roos F, Khoder W, Tsaur I, Nelson K, Bechstein WO, Haferkamp A, Blaheta RA, Sulforaphane inhibits proliferation and invasive activity of everolimus-resistant kidney cancer cells in vitro, 7 (2016) 85208–85219.

[12]. Calvo E, Schmidinger M, Heng DYC, Grünwald V, Escudier B, Improvement in survival end points of patients with metastatic renal cell carcinoma through sequential targeted therapy, Cancer Treat. Rev 50 (2016) 109–117. doi:10.1016/j.ctrv.2016.09.002. [PubMed: 27664394]

[13]. Krusch M, Salih J, Schlicke M, Kampa KM, Mayer F, Salih R, Krusch M, Salih J, Schlicke M, Baessler T, Kampa KM, Mayer F, Salih HR, The Kinase Inhibitors Sunitinib and Sorafenib Differentially Affect NK Cell Antitumor Reactivity In Vitro, (2017). doi:10.4049/jimmunol.0902404.

[14]. Bellmunt J, Pons F, Foreshew A, Fay AP, Powles T, Porta C, Bracarda S, Lampron ME, Cerbone L, Sternberg CN, Hutson TE, Choueiri TK, Sequential Targeted Therapy After Pazopanib Therapy in Patients With Metastatic Renal Cell Cancer : Ef fi cacy and Toxicity, Clin. Genitourin. Cancer 12 (2014) 262–269. doi:10.1016/j.clgc.2014.03.002. [PubMed: 24795159]

[15]. Hillen F, Griffioen AW, Tumour vascularization: Sprouting angiogenesis and beyond, Cancer Metastasis Rev. 26 (2007) 489–502. doi:10.1007/s10555-007-9094-7. [PubMed: 17717633]

[16]. Cheriyan VT, Alsaab HO, Sekhar S, Stieber C, Iyer AK, Rishi AK, A CARP-1 functional mimetic loaded vitamin E-TPGS micellar nano-formulation for inhibition of renal cell carcinoma, (2017).

[17]. Mcdonald PC, Dedhar S, Carbonic Anhydrase IX (CAIX) as a Mediator of Hypoxia-Induced Stress Response in Cancer Cells, (2014) 255–269. doi:10.1007/978-94-007-7359-2.

[18]. Jiang YD, Ren F, Zheng SB, Value of MN/CAIX in the diagnosis of renal cell carcinoma, Nan Fang Yi Ke Da Xue Xue Bao= J. South. Med. Univ 32 (2012) 412–414.

[19]. López CM, Esteban E, Berros JP, Pardo P, Astudillo A, Izquierdo M, Crespo G, Sanmamed M, Fonseca PJ, Mart\'\inez-Camblor P, Prognostic factors in patients with advanced renal cell carcinoma, Clin. Genitourin. Cancer 10 (2012) 262–270. [PubMed: 22959659]

[20]. Liao S-Y, Aurelio ON, Jan K, Zavada J, Stanbridge EJ, Identification of the MN/CA9 protein as a reliable diagnostic biomarker of clear cell carcinoma of the kidney, Cancer Res. 57 (1997) 2827–2831. [PubMed: 9230182]

[21]. Peña C, Lathia C, Shan M, Escudier B, Bukowski RM, Biomarkers predicting outcome in patients with advanced renal cell carcinoma: results from sorafenib phase III TARGET, Clin. Cancer Res. (2010) clincanres−−3343.

[22]. Choueiri TK, Cheng S, Qu AQ, Pastorek J, Atkins MB, Signoretti S, Carbonic anhydrase IX as a potential biomarker of efficacy in metastatic clear-cell renal cell carcinoma patients receiving sorafenib or placebo: analysis from the treatment approaches in renal cancer global evaluation trial (TARGET), in: Urol. Oncol. Semin. Orig. Investig, 2013: pp. 1788–1793.

[23]. Choueiri TK, Regan MM, Rosenberg JE, Oh WK, Clement J, Amato AM, McDermott D, Cho DC, Atkins MB, Signoretti S, Carbonic anhydrase IX and pathological features as predictors of

outcome in patients with metastatic clear-cell renal cell carcinoma receiving vascular endothelial growth factor-targeted therapy, BJ U Int. 106 (2010) 772–778.

[24]. Waheed A, Pastorekova S, Parkkila S, Rajaniemi H, Parkkila A, Kivela J, Pastorek J, Sly WS, Carbonic anhydrase inhibitor suppresses invasion of renal cancer cells in vitro, (2000).

[25]. Oosterwijk-Wakka JC, Kats-Ugurlu G, Leenders WPJ, Kiemeney LALM, Old LJ, Mulders PFA, Oosterwijk E, Effect of tyrosine kinase inhibitor treatment of renal cell carcinoma on the accumulation of carbonic anhydrase IX-specific chimeric monoclonal antibody cG250, BJU Int. 107 (2011) 118–125. [PubMed: 20346054]

[26]. Escudier B, Szczylik C, Porta C, Gore M, Treatment selection in metastatic renal cell carcinoma: expert consensus, Nat. Rev. Clin. Oncol 9 (2012) 327–337. [PubMed: 22473096]

[27]. Minn I, Koo SM, Lee HS, Brummet M, Rowe SP, Gorin A, Sysa-shah P, Lewis WD, Ahn H, Wang Y, Banerjee SR, Mease RC, Nimmagadda S, Mohamad E, Pomper MG, Yang X, [Cu] XYIMSR-06 : A dual-motif CAIX ligand for PET imaging of clear cell renal cell carcinoma, 7 (2016).

[28]. Muselaers CHJ, Stillebroer AB, Rijpkema M, Franssen GM, Oosterwijk E, Mulders PFA, Oyen WJG, Boerman OC, Anhydrase IX Monoclonal Antibody Girentuximab, (n.d.) 1035–1041. doi: 10.2967/jnumed.114.137356.

[29]. McDonald PC, Winum J-Y, Supuran CT, Dedhar S, Recent developments in targeting carbonic anhydrase IX for cancer therapeutics, Oncotarget. 3 (2012) 84–97. [PubMed: 22289741]

[30]. Krall N, Pretto F, Mattarella M, Neri D, Tc-Labeled Ligand of Carbonic Anhydrase IX Selectively Targets Renal Cell Carcinoma In Vivo, (n.d.) 943–950. doi:10.2967/jnumed. 115.170514.

[31]. Manuscript A, NIH Public Access, 2015. doi:10.1007/978-94-007-7359-2.

[32]. Brouwers AH, Carbonic Anhydrase IX Expression in Clear Cell Renal Cell Carcinoma and Normal Tissues : Experiences From (Radio) Immunotherapy Carbonic Anhydrase IX Expression in Clear Cell Renal Cell Carcinomas Negatively Correlates With the Proportion of the Granula, 26 (2017) 3808–3809. doi:10.1200/JCO.2008.17.6073.

[33]. Bhise K, Sau S, Alsaab H, Kashaw SK, Tekade RK, Iyer AK, Nanomedicine for cancer diagnosis and therapy: advancement, success and structure--activity relationship, Ther. Deliv 8 (2017) 1003–1018. [PubMed: 29061101]

[34]. Wickens JM, Alsaab HO, Kesharwani P, Bhise K, Amin MCIM, Tekade RK, Gupta U, Iyer AK, Recent advances in hyaluronic acid-decorated nanocarriers for targeted cancer therapy, Drug Discov. Today 22 (2016) 665–680. doi:10.1016/j.drudis.2016.12.009. [PubMed: 28017836]

[35]. Luong D, Kesharwani P, Alsaab HO, Sau S, Padhye S, Sarkar FH, Iyer AK, Folic acid conjugated polymeric micelles loaded with a curcumin difluorinated analog for targeting cervical and ovarian cancers, Colloids Surfaces B Biointerfaces. (2017).

[36]. Sau S, Alsaab HO, Kashaw SK, Tatiparti K, Iyer AK, Advances in antibody-drug conjugates: A new era of targeted cancer therapy, Drug Discov. Today 00 (2017). doi:10.1016/j.drudis. 2017.05.011.

[37]. Alsaab H, Alzhrani RM, Kesharwani P, Sau S, Boddu SHS, Iyer AK, Folate Decorated Nanomicelles Loaded with a Potent Curcumin Analogue for Targeting Retinoblastoma, Pharmaceutics. 9 (2017) 15.

[38]. Escudier B, Eisen T, Stadler WM, Szczylik C, Oudard S, Siebels M, Negrier S, Chevreau C, Solska E, Desai AA, Rolland F, Demkow T, Hutson TE, Gore M, Freeman S, Schwartz B, Shan M, Simantov R, Bukowski RM, Sorafenib in Advanced Clear-Cell Renal-Cell Carcinoma, N. Engl. J. Med 356 (2007) 125–134. doi:10.1056/NEJMoa060655. [PubMed: 17215530]

[39]. Zhang L, Bhasin M, Schor-Bardach R, Wang X, Collins MP, Panka D, Putheti P, Signoretti S, Alsop DC, Libermann T, Atkins MB, Mier JW, Goldberg SN, Bhatt RS, Resistance of renal cell carcinoma to sorafenib is mediated by potentially reversible gene expression, PLoS One. 6 (2011). doi:10.1371/journal.pone.0019144.

[40]. Cheriyan VT, Muthu M, Patel K, Sekhar S, Rajeswaran W, Larsen SD, Polin L, Levi E, Singh M, Rishi AK, CARP-1 functional mimetics are novel inhibitors of drug-resistant triple negative breast cancers, Oncotarget. 2 (2016) 73370–73388. doi:10.18632/oncotarget.12333.

[41]. Kawakami K, Yamamura S, Hirata H, Ueno K, Saini S, Majid S, Tanaka Y, Kawamoto K, Enokida H, Nakagawa M, others, 356 SECRETED FRIZZLED-RELATED PROTEIN-5 (SFRP-5) IS EPIGENETICALLY DOWNREGULATED AND FUNCTIONS AS A TUMOR SUPPRESSOR IN RENAL CELL CANCER, J. Urol 183 (2010) e141.

[42]. Yang Y, Lane AN, Ricketts CJ, Sourbier C, Wei MH, Shuch B, Pike L, Wu M, Rouault TA, Boros LG, Fan TWM, Linehan WM, Metabolic Reprogramming for Producing Energy and Reducing Power in Fumarate Hydratase Null Cells from Hereditary Leiomyomatosis Renal Cell Carcinoma, PLoS One. 8 (2013). doi:10.1371/journal.pone.0072179.

[43]. Almansour AI, Arumugam N, Suresh Kumar R, Mahalingam SM, Sau S, Bianchini G, Menéndez JC, Altaf M, Ghabbour HA, Design, synthesis and antiproliferative activity of decarbonyl luotonin analogues, Eur. J. Med. Chem 138 (2017) 932–941. doi:10.1016/j.ejmech.2017.07.027. [PubMed: 28753517]

[44]. Anjibabu R, Sau S, Reddy BJM, Banerjee R, Reddy BVS, Heteropoly acid catalyzed synthesis of 8-methyl-2-aryl/alkyl-3- oxabicyclo[3.3.1]non-7-ene derivatives through (3,5)-oxonium-ene reaction, Tetrahedron Lett. 54 (2013) 7160–7163.

[45]. Zhang N, Hong B, Zhou C, Du X, Chen S, Deng X, Duoerkun S, Li Q, Yang Y, Gong K, Cobalt Chloride-induced Hypoxia Induces Epithelial-mesenchymal Transition in Renal Carcinoma Cell Lines, Ann. Clin. Lab. Sci 47 (2017) 40–46. [PubMed: 28249915]

[46]. Shih J-W, Chiang W-F, Wu ATH, Wu M-H, Wang L-Y, Yu Y-L, Hung Y-W, Wang W-C, Chu C-Y, Hung C-L, others, Long noncoding RNA LncHIFCAR/MIR31HG is a HIF-1$α$ co-activator driving oral cancer progression, Nat. Commun 8 (2017) 15874. [PubMed: 28639619]

[47]. Wang Z, Sau S, Alsaab HO, Iyer AK, CD44 Directed Nanomicellar Payload Delivery Platform for Selective Anticancer Effect and Tumor Specific Imaging of Triple Negative Breast Cancer., Nanomedicine. (2018) #pagerange#. doi:10.1016/j.nano.2018.04.004.

[48]. Lin C, Chi B, Wong K, Chen H, Bian Z, Zhang G, Lu A, Yang Z, Pulmonary delivery of triptolide- loaded liposomes decorated with anti-carbonic anhydrase IX antibody for lung cancer therapy, Sci. Rep (2017) 1–12. doi:10.1038/s41598-017-00957-4. [PubMed: 28127051]

[49]. Gawde KA, Kesharwani P, Sau S, Sarkar FH, Padhye S, Kashaw SK, Iyer AK, Synthesis and characterization of folate decorated albumin bio-conjugate nanoparticles loaded with a synthetic curcumin difluorinated analogue, J. Colloid Interface Sci 496 (2017) 290–299. [PubMed: 28236692]

[50]. Sau S, Mondal SK, Kashaw SK, Iyer AK, Banerjee R, Combination of cationic dexamethasone derivative and STAT3 inhibitor (WP1066) for aggressive melanoma: a strategy for repurposing a phase I clinical trial drug, Mol. Cell. Biochem (2017) 1–18.

[51]. Sahu P, Kashaw SK, Jain S, Sau S, Iyer AK, Assessment of penetration potential of pH responsive double walled biodegradable nanogels coated with eucalyptus oil for the controlled delivery of 5-fluorouracil: In vitro and ex vivo studies, J. Control. Release 253 (2017) 122–136. doi:10.1016/j.jconrel.2017.03.023. [PubMed: 28322977]

[52]. Dal Corso A, Neri D, Linker stability influences the anti-tumor activity of acetazolamide-drug conjugates for the therapy of renal cell carcinoma, J. Control. Release 246 (2017) 39–45. doi: 10.1016/j.jconrel.2016.11.023. [PubMed: 27890855]

[53]. Shibata T, Kimura Y, Mori H, Ito S, Asaka Y, Oe S, Tanaka H, Takahashi T, Transthiocarbamoylation of Proteins by Thiolated, (2011). doi:10.1074/jbc.M111.308049.

[54]. Lv PC, Roy J, Putt KS, Low PS, Evaluation of a Carbonic Anhydrase IX-Targeted Near-Infrared Dye for Fluorescence-Guided Surgery of Hypoxic Tumors, Mol. Pharm 13 (2016) 1618–1625. doi:10.1021/acs.molpharmaceut.6b00065. [PubMed: 27043317]

[55]. Hoogstins CES, Tummers QRJG, Gaarenstroom KN, De Kroon CD, Trimbos JBMZ, Bosse T, Smit VTHBM, Vuyk J, Van De Velde CJH, Cohen AF, Low PS, Burggraaf J, Vahrmeijer AL, A novel tumor-specific agent for intraoperative nearinfrared fluorescence imaging: A translational study in healthy volunteers and patients with ovarian cancer, Clin. Cancer Res. 22 (2016) 2929–2938. doi:10.1158/1078-0432.CCR-15-2640. [PubMed: 27306792]

[56]. I.C. on Harmonisation, Ich Harmonised Tripartite Guideline Validation of Analytical Procedures :, ICH Harmon. Tripart. Guidel. Valid. Anal. Proced. TEXT Methodol. Q2(R1) Step4 (2005). doi:10.1017/CBO9781107415324.004.

[57]. Zhang Z, Tan S, Feng SS, Vitamin E TPGS as a molecular biomaterial for drug delivery, Biomaterials. 33 (2012) 4889–4906. doi:10.1016/j.biomaterials.2012.03.046. [PubMed: 22498300]

[58]. Dong K, Liu Z, Li Z, Ren J, Qu X, Hydrophobic anticancer drug delivery by a 980 nm laser-driven photothermal vehicle for efficient synergistic therapy of cancer cells in vivo, Adv. Mater. 25 (2013) 4452–4458. [PubMed: 23798450]

[59]. Pastorekova S, Carbonic anhydrase IX is a clinically significant tissue and serum biomarker associated with renal cell carcinoma, Oncol. Lett (2012). doi:10.3892/ol.2012.1001.

[60]. Bao B, Groves K, Zhang J, Handy E, Kennedy P, Cuneo G, Supuran CT, Yared W, Rajopadhye M, Peterson JD, In Vivo Imaging and Quantification of Carbonic Anhydrase IX Expression as an Endogenous Biomarker of Tumor Hypoxia, PLoS One. 7 (2012). doi:10.1371/journal.pone.0050860.

[61]. Soyupak B, Erdo\ugan \cSeyda, Ergin M, Seydao\uglu G, Kuzgunbay B, Tansu\ug Z, CA9 expression as a prognostic factor in renal clear cell carcinoma, Urol. Int 74 (2005) 68–73. [PubMed: 15711113]

[62]. Uemura H, Fujimoto K, Tanaka M, Yoshikawa M, Hirao Y, Uejima S, Yoshikawa K, Itoh K, A phase I trial of vaccination of CA9-derived peptides for HLA-A24-positive patients with cytokine-refractory metastatic renal cell carcinoma, Clin. Cancer Res. 12 (2006) 1768–1775. doi:10.1158/1078-0432.CCR-05-2253. [PubMed: 16551861]

[63]. Dong K, Ju E, Liu J, Han X, Ren J, Qu X, Ultrasmall biomolecule-anchored hybrid GdVO 4 nanophosphors as a metabolizable multimodal bioimaging contrast agent, Nanoscale. 6 (2014) 12042–12049. [PubMed: 25185795]

[64]. Puliyappadamba VT, Wu W, Bevis D, Zhang L, Polin L, Kilkuskie R, Finley RL, Larsen SD, Levi E, Miller FR, Wali A, Rishi AK, Antagonists of Anaphasepromoting Complex (APC)-2-Cell Cycle and Apoptosis Regulatory Protein (CARP)-1 interaction are novel regulators of cell growth and apoptosis, J. Biol. Chem 286 (2011) 38000–38017. doi:10.1074/jbc.M111.222398. [PubMed: 21903591]

[65]. Muthu M, Cheriyan VT, Rishi AK, CARP-1/CCAR1: a biphasic regulator of cancer cell growth and apoptosis., Oncotarget. 6 (2015) 6499–510. doi:10.18632/oncotarget.3376. [PubMed: 25894788]

[66]. Hsieh JJ, Manley BJ, Khan N, Gao J, Carlo MI, Cheng EH, Overcome tumor heterogeneity-imposed therapeutic barriers through convergent genomic biomarker discovery: a braided cancer river model of kidney cancer, in: Semin. Cell Dev. Biol, 2017: pp. 98–106.

[67]. Molina AM, Feldman DR, Voss MH, Ginsberg MS, Baum MS, Brocks DR, Fischer PM, Trinos MJ, Patil S, Motzer RJ, Phase 1 trial of everolimus plus sunitinib in patients with metastatic renal cell carcinoma, Cancer. 118 (2012) 1868–1876. doi:10.1002/cncr.26429. [PubMed: 21898375]

[68]. Hsieh JJ, Cheng EH, A braided cancer river connects tumor heterogeneity and precision medicine, Clin. Transl. Med 5 (2016) 42. doi:10.1186/s40169-016-0123-4. [PubMed: 27766604]

[69]. Zajac E, Schweighofer B, Kupriyanova TA, Juncker-Jensen A, Minder P, Quigley JP, Deryugina EI, Angiogenic capacity of M1- and M2-polarized macrophages is determined by the levels of TIMP-1 complexed with their secreted proMMP-9, Blood. 122 (2013) 4054–4067. doi:10.1182/blood-2013-05-501494. [PubMed: 24174628]

[70]. Alsaab HO, Sau S, Alzhrani R, Tatiparti K, Bhise K, Kashaw SK, Iyer AK, PD-1 and PD-L1 Checkpoint Signaling Inhibition for Cancer Immunotherapy: Mechanism, Combinations, and Clinical Outcome, Front. Pharmacol 8 (2017) 1–15. doi:10.3389/fphar.2017.00561. [PubMed: 28149278]

[71]. Bally APR, Lu P, Tang Y, Austin JW, Scharer CD, Ahmed R, Boss JM, NF-κB Regulates PD-1 Expression in Macrophages, J. Immunol. 194 (2015) 4545–4554. doi:10.4049/jimmunol.1402550. [PubMed: 25810391]

[72]. Zhang RR, Schroeder AB, Grudzinski JJ, Rosenthal EL, Warram JM, Pinchuk AN, Eliceiri KW, Kuo JS, Weichert JP, Beyond the margins: real-time detection of cancer using targeted fluorophores, Nat. Rev. Clin. Oncol 14 (2017) 347–364. doi:10.1038/nrclinonc.2016.212. [PubMed: 28094261]

[73]. Wilhelm S, Tavares AJ, Dai Q, Ohta S, Audet J, Dvorak HF, Chan WCW, Analysis of nanoparticle delivery to tumours, Nat. Rev. Mater 1 (2016). doi:10.1038/natrevmats.2016.14.

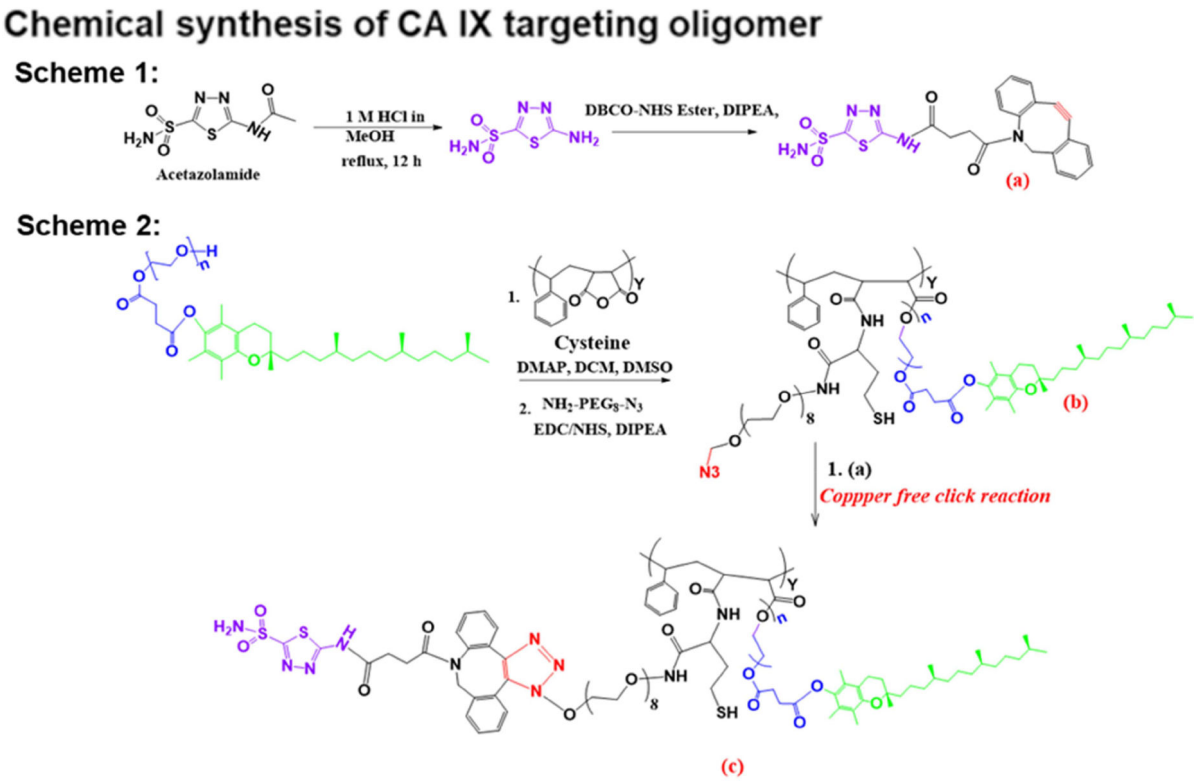

Figure 1:

The general procedure for acetazolamide-oligomer (CA IX-SMA-TPGS) synthesis is shown. The final '*click*' reaction product, compound c has been used to encapsulate C4.16 or to conjugate with S0456 or Rhodamine dye with -SH functional group to obtain CA IX-oligomer.

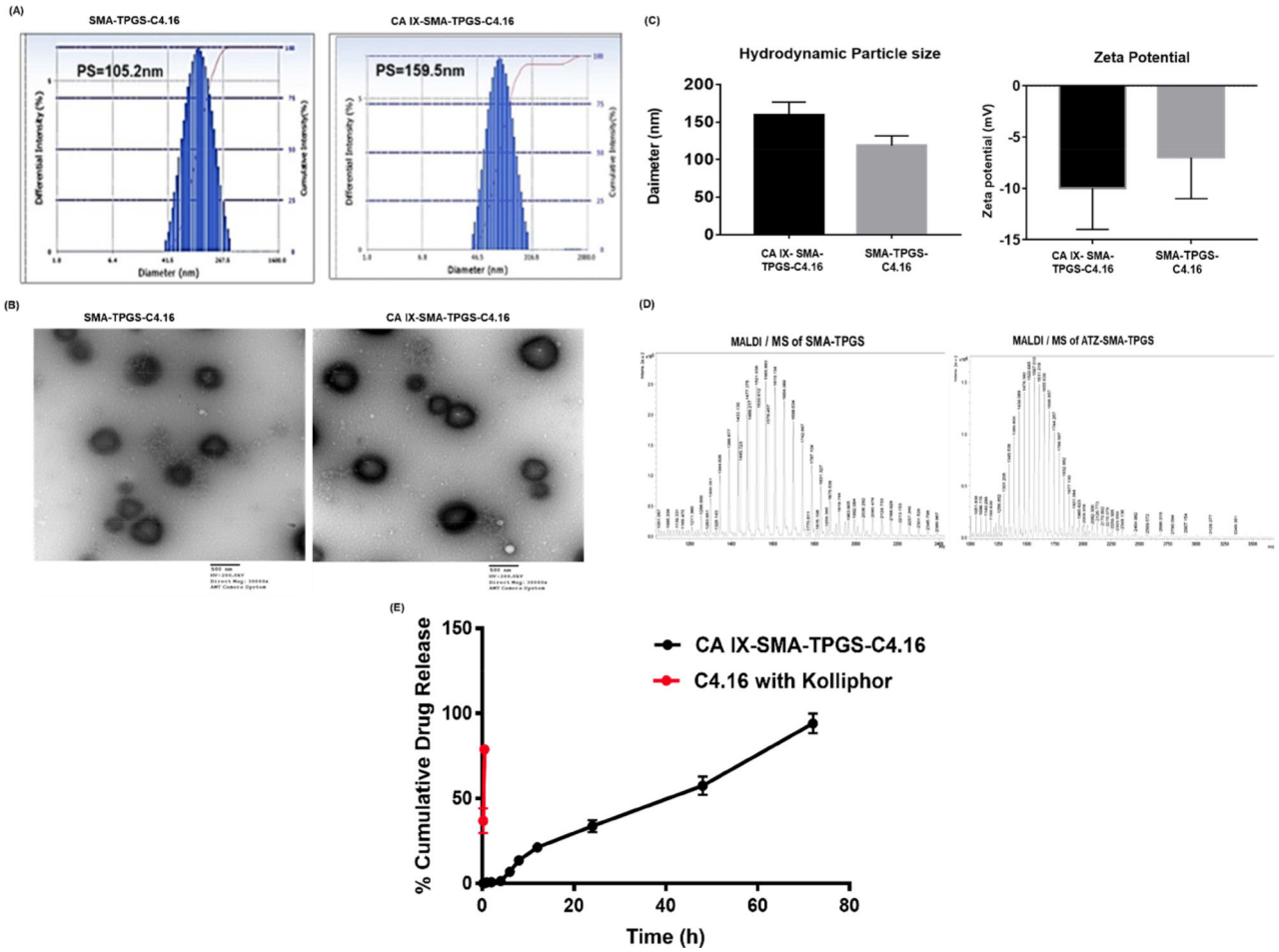

Figure 2. Nanoparticle formulation and characterization.

(A) Hydrodynamic size of targeted non-targeted SMA-TPGS-C4.16 and hypoxia targeting CA IX-SMA-TPGSC4.16 NP are shown. **(B)** The transmission electron micrographs shows the morphology of non-targeted and targeted NP. (**C)** The zeta potential or surface charge on the NPs by Dynamic Light Scattering (DLS) is shown. (Representative histogram of hydrodynamic particle size and zeta potential (n=3). **(D)** MALDI/MS analysis of CA IXSMA-TPGS and SMA-TPGS are shown. The increment of molecular weight in CA IXSMA-TPGS (m/z 3126) compared to SMA-TPGS (m/z 2399), and their corresponding fragmented peaks indicates the successful conjugation of ATZ to the SMA-TPGS polymer. (**E**) In vitro drug release kinetics of CAIX-SMA-TPGS-C4.16 in PBS indicates that the sustained release of C4.16 from the CAIX-SMA-TPGS-C4.16 NP as compared to free C4.16 with excipient, such as Kolliphor in PBS is shown.

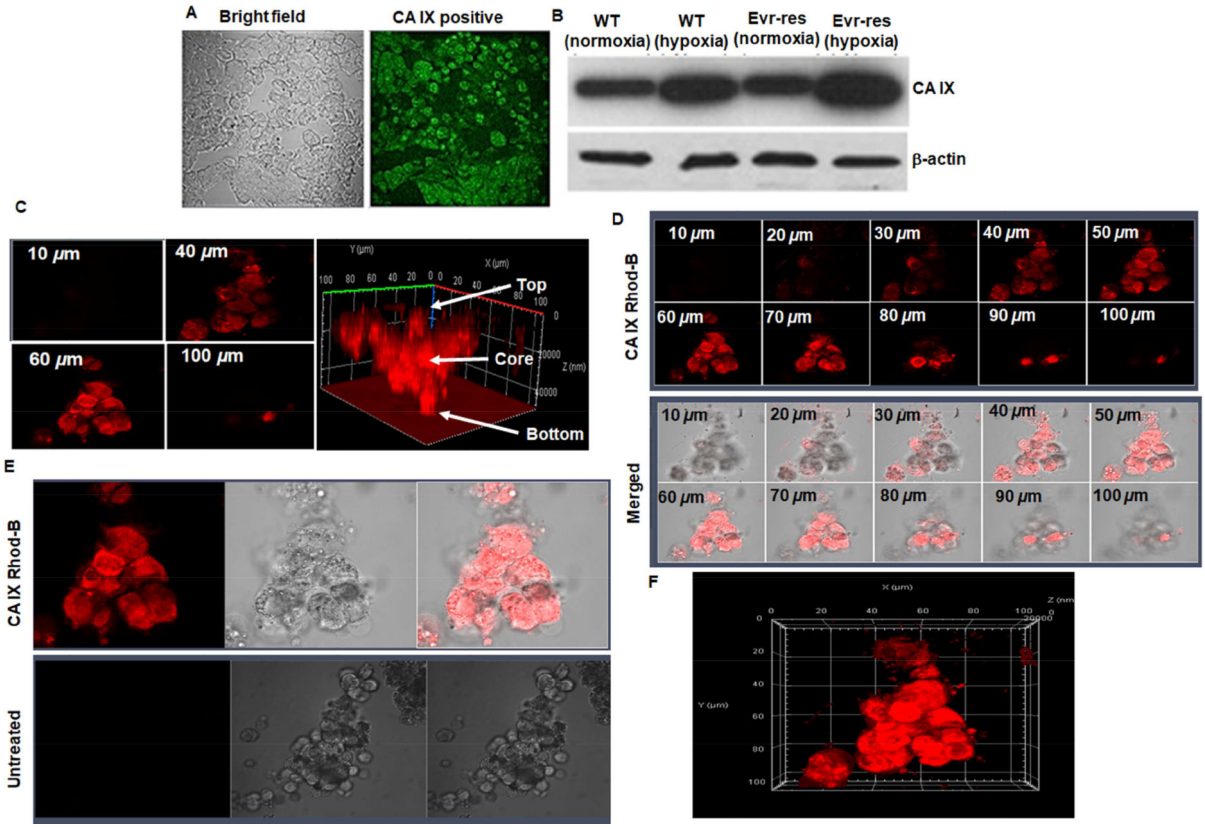

Figure 3. Hypoxia induced CA IX-overexpression in A498 cells and tumors to enable tumor core penetration of CA IX oligomer.

(A) Immunohistochemistry of CA IX-positive A498 RCC tumor xenografts collected from tumor tissue section is shown. The intense bright green fluorescence indicates the rationale for choosing CA IX as an excellent biomarker for RCC specific payload delivery. **(B)** Western blot detection of CA IX protein in A498 and EV-A498 RCC cells lysates after normoxia and hypoxia (treated with cobalt chloride for 72 h) are shown. The fold up-regulation of CA IX expression in hypoxic WT and EV-res A498 RCC cells compared to normoxia provides a solid foundation for delivering the payload into oxygen-deprived regions and the hypoxic core of RCC tumor. **(C)** 3D spheroid uptake studies of hypoxia targeted-oligomer (CA IX Rhod-B). Confocal microscope images of CA IX Rhod-B treated hypoxic A498 spheroid indicates tumor matrix penetration of CA IX-oligomer. The untreated and treated spheres were then photographed as noted in the methods section. Z-stacking of the spheroid clearly indicates that fluorescence intensity is superior in 40–60 μm section (core) as compared to 10 or 100 μm (periphery). The highest fluorescence intensity at the center (as indicated by arrow) of 3D- plot suggests that CA IX-Rhod oligomer is highly efficient to reach deep into the core of the tumor spheroid. **(D)** Z-stacking of the spheroid at different sections from 10–100μm with CA IX targeted formulations also reveals similar findings as noted for the 40–60 μm that had superior fluorescence intensity. Figure **(E)** shows the untreated control experiments in comparison with CA IXRhod oligomer and Figure (**F**) shows the overall shape and morphology of the spheroid along the three dimensional (x, y, and z) axis.

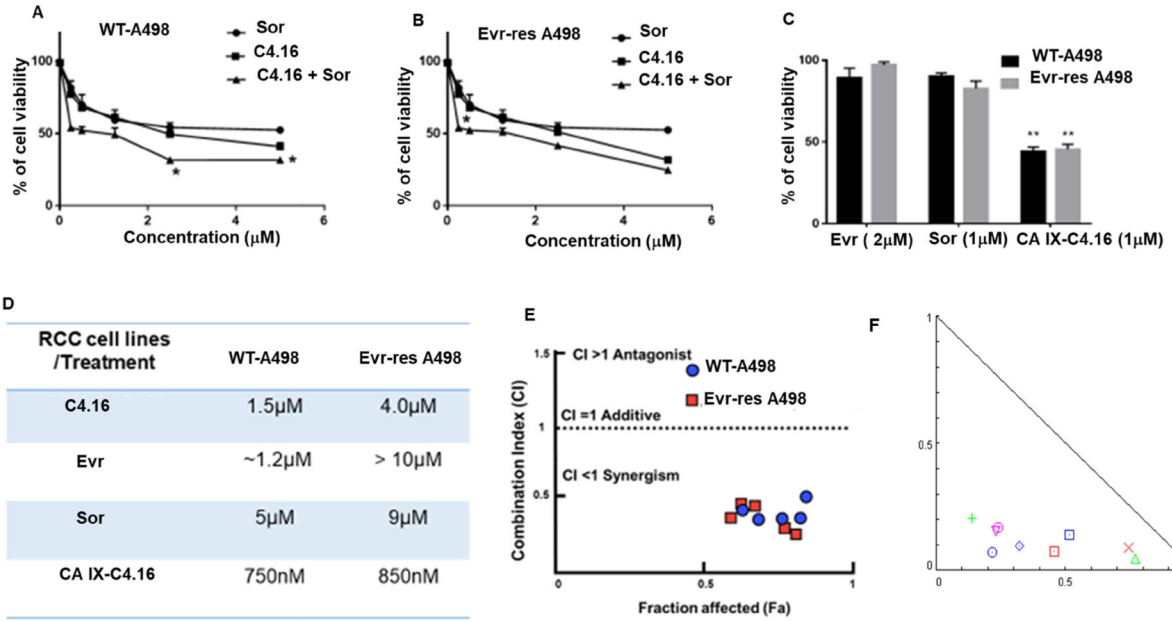

RCC cell lines /Treatment	WT-A498	Evr-res A498
C4.16	1.5μM	4.0μM
Evr	~1.2μM	> 10μM
Sor	5μM	9μM
CA IX-C4.16	750nM	850nM

Figure 4. C4.16 and CA IX-C4.16 are more efficient in inhibiting the growth of WT and Evr-res A498 cells.

In vitro cytotoxicity assay of C4.16 and Sor on **(A)** WT and **(B)** Evr-res A498 indicates C4.16 was more potent than the FDA approved drug, Sor and combining both drugs C4.16+Sor demonstrated significantly lower cell viability. **(C)** The results also showed that CA IX-C4.16 is more effective in inhibiting the growth of A498 (WT and Evr-res) RCC cell lines compared to Sor and Evr and support the notion that C4.16 is more potent than FDA approved drugs in the RCC model. **(D)** Summary of IC_{50} value for all the tested drugs with the tested RCC cell lines are shown in a tabular fashion. The data in the IC_{50} columns represent the mean of three independent experiments. Indicated A498 WT and their respective Evr-res A498 cells were either untreated (control) or treated with a noted dose of C4.16, Sor, Evr, and CA IX-C4.16 for 48 h. **(E)** High synergistic CI value of C4.16 in combination with Sor supports the hypothesis of selecting the combination to treat RCC for reversing the drug resistance. This data builds a rationale for using hypoxic core penetrating CA IX-C4.16+Sor to sensitize the drug resistant RCC. **(F)** Isobologram of CA IX-C4.16+Sor suggests high synergism combination treatment in RCC cells.

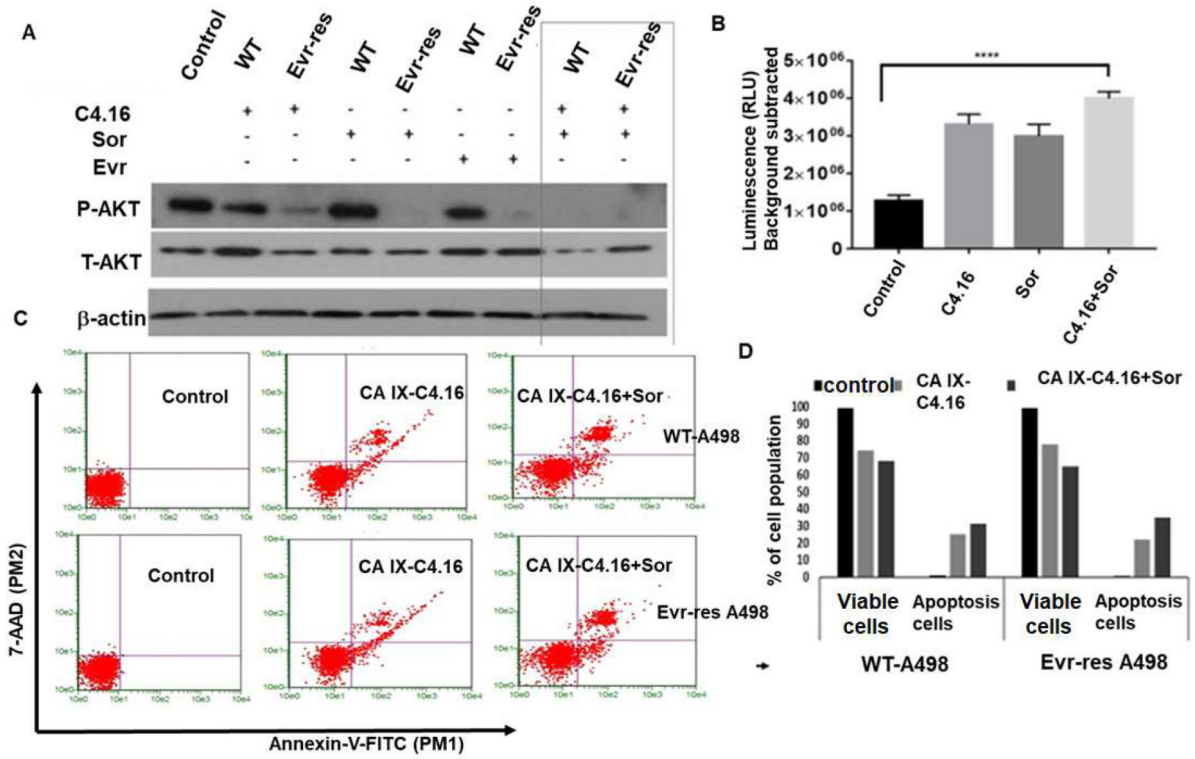

Figure 5. (A) Molecular mechanism of cell death and resurrection of apoptosis:
Western blot analysis clearly indicates that C4.16+Sor combination completely wiped out P-AKT level both in WT and Evr-res A498 cells. Cell were either kept untreated (control, C) or treated with Evr, Sor, C4.16 or C4.16+Sor. **(B)** Up-regulation of caspase 7/9 with (C4.16+Sor) treatment in Evr-res A498 cells indicates effective induction of apoptosis to drug resistant cells as compared to control or individual treatment. The results support the notion that (C4.16+Sor) combination is more effective in resurrecting apoptosis mediated cell death. Data represent mean ± SD, n=3 per group, ****$p<0.01$ vs. control. **(C)** Apoptosis analysis of WT and Evr-res A498 cell by FACS using dual Annexin-V and 7-AAD staining. The data indicates CA IX-C4.16+Sor is superior in inducing apoptosis as compared to control; CA IX-C4.16 NP treated cells. **(D)** Histogram columns of both viable cells and apoptotic cells indicates that CA IX-C4.16 + Sor has more % apoptotic cell compared to CA IX-C4.16 alone which support our hypothesis of the synergism in RCC cell killing.

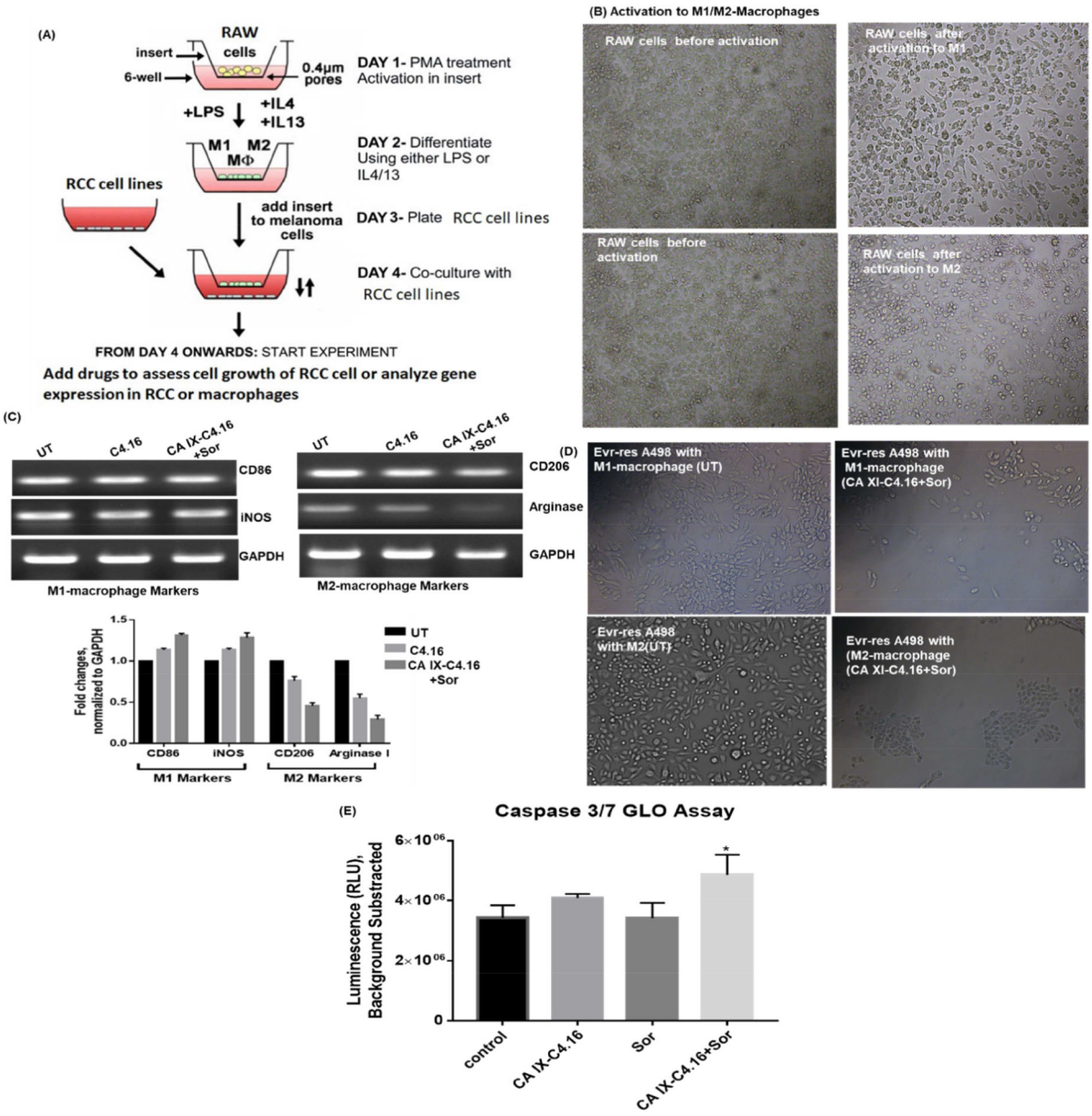

Figure 6. Reprogramming macrophages with CA IX-C4.16+Sorafenib treatment.

(A) Schematic representation of the procol is shown. Raw-264.7 cells were placed into the insert. Then, cells were polarized to M1-macrophage using IFN-γ and LPS, and to M2-macrophage using IL-4 recombinant protein. The scheme was modified from the original protocol by Smith *et al.* **(B)** Change of morphology of M1 and M2 macrophages supports the polarization of Raw-264.7. **(C)** RT-PCR data clearly demonstrates the upmodulation of the tumoricidal M1-macrophage marker (CD86, iNOS) and downmodulation of the tumorigenic M2-macrophage marker (CD206, Arginase I) in CA IXC4.16+Sor as compared to control and C4.16. The macrophage reprogramming ability of CA IX-targeting NP builds a rational of using (CA IX-C-4.16+Sor) as a potent antitumor immune-stimulatory agent for RCC. **(D)** Change of morphology and reduction of Evr-res A498 density in M1-macrophage and Evr-res A498 co-cultured condition, treated with CA XI+Sor suggests activated M1-

macrophage mediated RCC cell death. (**E**) Treatment of CA IX+Sor educate the Raw-264.7 in inducing caspase 3/7 mediated apoptosis of Evr-res A498.

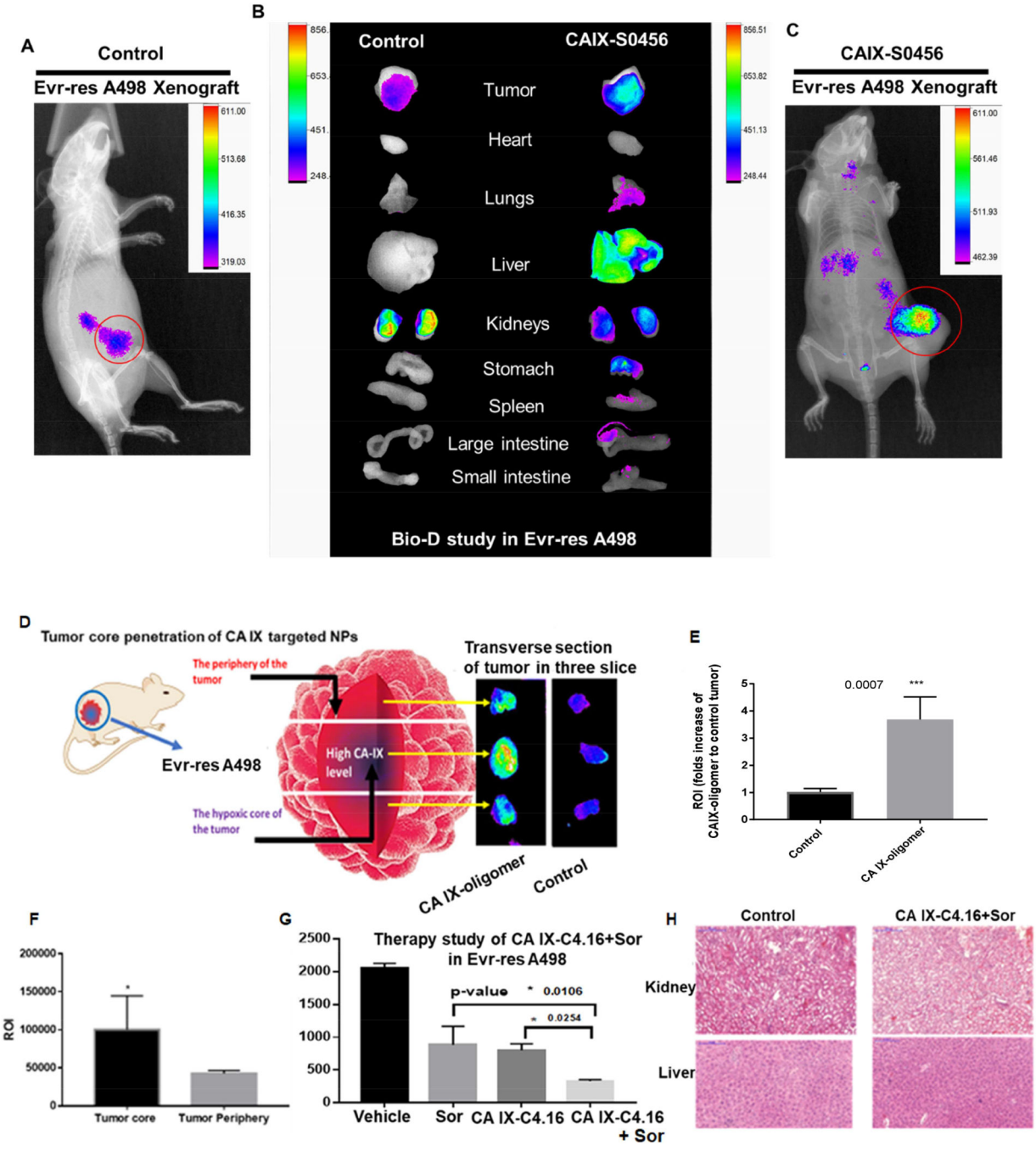

Figure 7: Superior tumor specificity of CA IX-oligomer and combination antitumor efficacy study in Evr-res A498 xenograft RCC model.

(A and C) Superior tumor accumulation of CAIX oligomer (CA IX-S0456) as compared to control (S0456) in Evrres A498 tumor xenograft model is shown. **(B)** Biodistribution (Bio-D) study of CA IXS0456 showed superior tumor specificity and low non-specific liver uptake in Evr-res A498 tumor bearing mice. The control, S0456 showed poor tumor accumulation with high off-target activity. (**D**) Further to demonstrate the tumor core penetration of NIR dye, the isolated Evr-res A498 tumor was transversely sectioned into 3

parts; the brightest fluorescence intensity at the middle (core) section confirmed the excellent hypoxic tumor core penetration ability of CA IX-S0456 compared with non targeted control. (**E**) Significantly high tumor accumulation (more than 3-fold) of CA IX-oligomer compared to control suggests the high tumor specificity of the oligomer. (**F**) Quantification of fluorescent ROI indicates CA IX-oligomer had significantly high tumor core penetration and accumulation as compared to its periphery. The results suggest the importance of CA IX-oligomer in selective RCC tumor targeting ability. **(G)** CA IXC4.16+Sor showed significant tumor growth inhibition compared to vehicle(control), Sor, and CA IX-C4.16 in Evr-res A498 xenograft tumor. The remarkable tumor growth suppression of combination therapy supports the rationale of using CA IX targeting nano-formulation as the delivery vehicle of potent drugs such as C4.16. The data is represented as average values from four animals in the respective group, bars, SE, significant where *$p<0.05$ vs. Control. **(H)** Histopathologic (H&E staining) examination was done to determine the toxicity of therapeutic drugs on livers and kidneys at the end of the experiments. The **i**mages indicate that there is no significant sign of necrosis or loss of tissue architectural in vehicle control and CA IX-C4.16+Sor treated tissues indicating safety of the formulations.

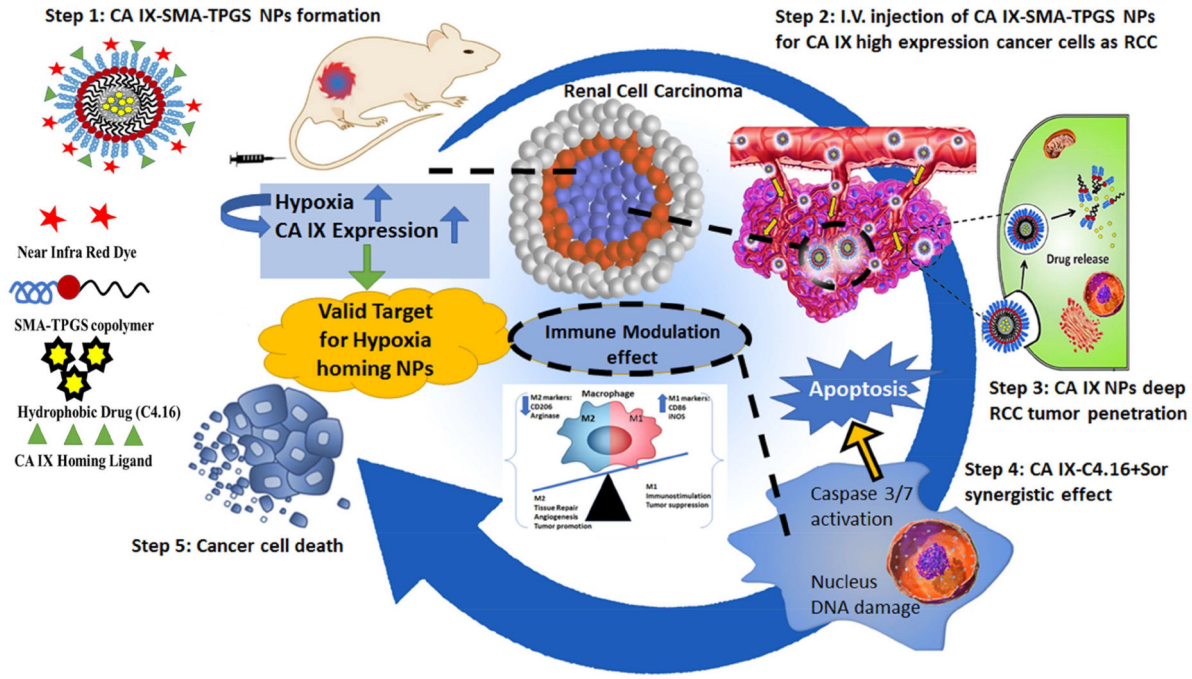

Scheme 1:

Summary of tumor hypoxia directed nanotherapy in combination with Sorafenib for achieving multiple benefits against cancer, such as reversing drug resistance, inducing apoptosis and reprogramming macrophages.

Table 1

Characterization of Nanoparticles.

Sample	CMC (mg/ml)	Hydrodynamic size (nm)	PDI	Zeta potential (mV)	EE (%)
CA IX-SMA-TPGS-C4.16 (Targeted)	0.021	159.5±20nm	0.094±0.05	−10.21±4	75.5±12
SMA-TPGS-C4.16 (non-targeted)	0.010	105.2±31nm	0.165±0.07	−7.86±4	85±9.8

Abbreviations: C4.16, CARP-1 Functional Mimetics; SMA, styrene maleic acid; TPGS, d-α-tocopheryl polyethylene glycol succinate; ATZ, Acetazolamide; CMC, critical micelle concentration; PDI, polydispersity index; EE, encapsulation efficiency.